PB 189 283

ELECTRON MICROPROBE X-RAY ANALYSIS OF ATMOSPHERIC AEROSOL PARTICLES

Advanced Metals Research Corporation
Burlington, Massachusetts

1969

Distributed ... 'to foster, serve
and promote the nation's
economic development
and technological
advancement.'

CLEARINGHOUSE
FOR FEDERAL SCIENTIFIC AND TECHNICAL INFORMATION

U.S. DEPARTMENT OF COMMERCE/National Bureau of Standards

This document has been approved for public release and sale.

PB189283

Electron Microprobe X-ray Analysis of Atmospheric Aerosol Particles

for

Department of Health, Education and Welfare
Consumer Protection and Environmental Health Service

Contract No. CPA 22-69-26

Period Covered: December 1, 1968 to August 31, 1969

AMR

Research and Development
- MATERIALS RESEARCH
- X-RAY ANALYSIS
- ELECTRON BEAM MICROANALYSIS
- INSTRUMENTATION

ADVANCED METALS RESEARCH CORPORATION

149 MIDDLESEX TURNPIKE • BURLINGTON, MASSACHUSETTS 01803

Reproduced by the
CLEARINGHOUSE
for Federal Scientific & Technical
Information Springfield Va. 22151

95

Electron Microprobe X-ray Analysis of
Atmospheric Aerosol Particles

for

Department of Health, Education and Welfare

Consumer Protection and Environmental Health Service

Contract No. CPA 22-69-26

Period Covered: December 1, 1968 to August 31, 1969

ABSTRACT

Electron microprobe analysis was applied to the chemical identification of the airborne particles characteristic of air pollution contaminants. A conventional AMR Electron Microprobe and a Philips EM200 Electron Microscope equipped with an AMR X-ray Spectrometer attachment were employed to investigate size-fractioned samples of laboratory generated aerosol particles of $Na\,Cl$ and $Zn\,(NH_4)_2\,(SO_4)_2$, as well as specific pollution sources, e.g. Los Angeles Smog and Auto Exhaust. The effect of instrument variables, including electron beam size, acceleration potential, and beam current was determined for particles ranging in size from 3μ to 0.5μ.

X-ray Spectral Patterns obtained from Los Angeles Smog particles are presented and inherent limitations in the analytical technique are also discussed.

Scanning Electron Microscopy was employed as a supplement to conventional Electron Microscopy and was found to furnish valuable information on the nature of the particulates.

microns

TABLE OF CONTENTS

Page

Abstract i

List of Illustrations iii

List of Tables v

I. Introduction 1

II. Experimental Procedure 4

A. Experimental Equipment 4

1. Electron Beam Microanalyzer 4
2. AMR X-ray Spectrometer Attachment for the Electron Microscope 6
3. Scanning Electron Microscopy 9

B. Sample Preparation 10

III. Results and Discussion 13

A. Optimization of Instrumental Parameters 13

1. Determination of beam current as a function of beam size 13
2. Effect of Increasing Electron Acceleration Potential 16
3. Conversion of X-ray Intensity to Concentration 18
4. Summary of Instrument Optimization in Relation to Small Particle Analysis 20

B. Studies of Laboratory Test Aerosols 21

1. Sodium Chloride 22
2. Zinc Ammonium Sulfate 22
   a. Current Density vs Beam Size 23
   b. X-ray Intensity vs Acceleration Potential 23
   c. X-ray Intensity vs Beam Diameter 31
   d. Summary 31

TABLE OF CONTENTS CONTINUED

Page

C. Atmospheric Samples 32
   1. Electron Beam Microanalysis 32
   2. Electron Microscopy/Electron Beam Microanalysis 34
   3. Scanning Electron Microscopy 65
D. Auto Exhaust Samples 66
E. Ni film specimens 71
IV. Future Analytical Systems 76
References 77

LIST OF ILLUSTRATIONS

Figures		**Page**
1 (a)	AMR Electron Beam Microanalyzer	5
1 (b)	AMR X-ray Spectrometer Attachment mounted on Philips EM 200 Electron Microscope	7
2	Electron Beam Current as a Function of Beam Size	17
3	Spectral Pattern from 2μ Diameter FeAl Silicate Particle employing a 2μ Diameter Beam	38
4	Spectral Pattern from 2μ Dia. FeAl Silicate Particle employing a 3μ Dia. Beam	39
5	Spectral Pattern from a 2μ Dia. FeAl Silicate Particle employing a 4μ Dia. Beam	40
6	Spectral Pattern from a 2μ Dia. FeAl Silicate Particle employing a 5μ Dia. Beam	41
7	Spectral Pattern from a 4μ Ca rich Particle	42
8	Spectral Pattern from a 1μ Ca rich Particle	43
9	Spectral Pattern from a 5μ Ca rich Particle	44
10	Spectral Pattern from a 3μ Particle containing Fe, Mg, Ti, Ca and Si	45
11	Spectral Pattern from a 4μ Particle containing Fe, Mg, Ti, Ca and Si	46
12	Spectral Pattern from a 1.5μ Al rich Particle	47
13	Spectral Pattern from a 5μ Particle rich in Ca, Cl, Zn and S	48
14	Spectral Pattern from a 5μ Particle containing Fe, Ca, Al, and Si	49
15	Spectral Pattern from 2.5μ dia. spherical particles containing Fe, Al and Si	50

LIST OF ILLUSTRATIONS CONTINUED

Figures		Page
16	Spectral Pattern from a 4μ Particle containing Fe, Al, K and Si	51
17	Spectral Pattern from a Particle containing Al and Si	52
18	Spectral Pattern from a 1μ Ca rich Particle	53
19	Spectral Pattern from a 0.5-1μ Fe rich Particle	54
20	Spectral Pattern from a 2μ Particle rich in Al and Si	55
21	Spectral Pattern from a 2μ Ca rich Particle	56
22	Spectral Pattern from a 1μ dia. Fe rich sphere	57
23	Spectral Pattern from a 2.5μ Particle	58
24	Spectral Pattern from a 1μ Particle	59
25	Spectral Pattern from a 1μ dia. Particle	60
26	Spectral Pattern from a 0.5μ Fe rich Particle	61
27	Scanning Electron Microscopy of Air Pollution Sample	67
28	Scanning Electron Microscopy of Air Pollution Sample	69
29	Scanning Electron Microscopy of Ni Film on Nitrocellulose	72
30	Scanning Electron Microscopy of Ni Film on Nitrocellulose	73
31	Scanning Electron Microscopy of Ni Film on Nitrocellulose	74
32	Scanning Electron Microscopy of Ni Film on Nitrocellulose	75

LIST OF TABLES

Table		Page
1	Typical Particulate Collections with the Battelle Cascade Impactor	11
2	Maximum Allowable Emission for Philips EM-200 Electron Gun	15
3	Beam Current as a Function of Electron Acceleration Potential	19
4	Effect of Beam Size and Acceleration Potential on Zn Kα X-ray Intensity from a 3μ Particle of Zn $(NH_4)_2(SO_4)_2$	24
5	Effect of Beam Size and Acceleration Potential on ZnKα X-ray Intensity from a 2μ Particle of $Zn(NH_4)_2(SO_4)_2$	25
6	ZnKα Intensity Versus Beam Diameter at 80KV for Sub-Micron Particles of $Zn(NH_3)_2(SO_4)_2$	26
7	Current Density as a Function of Acceleration Potential	27
8	ZnKα X-ray Intensity Per Microampere of Beam Current from a 3μ Particle of $Zn(NH_3)_2(SO_4)_2$	28
9	ZnKα X-ray Intensity per Microampere of Beam Current from a 2μ Particle of $Zn(NH_3)_2(SO_4)_2$	29
10	ZnKα X-ray Intensity per Microampere of Beam Current at 80KV from Sub-Micron Particles of $Zn(NH_3)_2(SO_4)_2$	30
11	Summary of Electron Beam Microanalysis of Particles on Stage 3	33
12	Si Kα X-ray Intensity vs. Beam Size for a 2μ Diameter Los Angeles Smog Particle	35
13	SiKα X-ray Intensity vs. Beam Size for a 1μ Diameter Los Angeles Smog Particle	36
14	Major Element Present in Atmospheric Aerosol Collection	63

I. Introduction

The effective control of atmospheric pollutants requires the capability of analyzing the airborne particles which are of significance in air pollution. As a result, interest in the application of the technique of Electron Microprobe X-ray Analysis has been stimulated.

In 1959, under contract to Tracer Lab/Keleket, AMR initiated the application of the electron microprobe to the study of fine aerosol particles. Hundreds of fine particles ranging in size from 3 to 20μ, collected as debris from nuclear explosions were analyzed. A simple technique was developed which consisted of adhering the particles to a disc of high purity, polished beryllium with a droplet of nitrocellulose. Since the Be characteristic X-rays are too soft to be detected by X-rays, the spectrum which was excited exclusively identified the elements present in the particle. During this period, the electron microprobe was employed to analyze the chemistry of individual particulates (1-3μ) as well as dense deposits of collections made by high altitude balloons, U-2 Jet Aircraft and at high altitude ground levels in Greenland.

In 1962, the electron microprobe technique was extended to the chemical analysis of particles ranging in size from 0.1 to 2μ. These analyses were performed at AMR by inserting electron microscopy grids into the microprobe. Although successful, frequent excursions from the electron microscope to the electron microprobe were required to locate particles.

To facilitate the analysis of small particles (down to 0.1μ in size), a combined electron microscope/electron microprobe was developed. This instrument called the AMR Probescope, was specifically designed for small particle analysis and is in essence an electron microprobe with the optics and magnification capability of an electron microscope. The samples employed in this instrument are typically those employed in electron microscopy, e.g. extraction replicas, powder dispersions, thin films, etc. Equipped with an X-ray Spectrometer, the instrument is capable of analyzing the X-rays produced in a sample while simultaneously viewing the sample at 20,000X.

An alternative method for the analysis of small particles was made possible by the development of an X-ray spectrometer attachment. This instrument attaches to the rotating tilting stage of a Philips EM200 electron microscope. Both dispersive and non-dispersive X-ray detection techniques are available with this device. As a result, this instrument provides an analytical capability similar to that provided by the probescope. The latter two instruments are superior to the electron microprobe analyzer for the application of small particle analysis. This superiority is not a result of any increase in analytical capability compared to microprobe, but rather in the fact that the samples can be viewed at high magnifications. As a result, the beam can be precisely positioned on the particle, and the particle shape and size can be recorded photographically. Any changes in particle morphology during electron beam bombardment resulting from melting, volatilization, loss of waters of hydration, or decomposition can be immediately ascertained. Since viewing in the microprobe is limited to low magnifications (∿300X), these effects can not be observed.

Pertinent to the discussion of sample viewing, the scanning electron microscope should be mentioned. This instrument provides an image of the specimen which is far superior in depth of field and resolution to that furnished by light microscopy. Although it lacks the resolution of conventional electron microscopy, it is quite adequate for viewing particles in the size range of interest (0.1 to 1 micron). Moreover, it provides an image of the sample which is three dimensional in quality compared to the flat, shadow-graphs observed in conventional electron microscopy.

Although the electron microprobe and related instruments have already been used to study very fine particles in the micron and sub-micron size range collected from various upper atmosphere or aqueous sources, no serious study has been undertaken to date in the area of air pollution. The purpose of this investigation is to determine suitable sample preparation procedures, proper choice of substrates, and the effects of experimental variables on the analytical capability of this technique. To accomplish this end, the effect of electron accelerating potential, electron beam size, and incident electron beam current on the production of characteristic X-rays from particles varying in size from 0.2μ to 3μ was investigated. Test aerosol particles of sodium chloride and zinc ammonium sulfate were employed in this study. Employing the results obtained from this work, instrument parameters were optimized for the chemical analysis of representative samples of atmospheric aerosol pollutants and auto exhaust residues. These particles had been collected employing a Batelle Cascade Impactor and hence consisted of samples which were grouped in different size ranges. Particles were characterized according to their major chemical constituents.

Finally, thin films of Ni (approximately 1000A° thick) vacuum evaporated on nitrocellulose substrates and supported on Cu electron microscope grids which were subjected to fine mists of sulfuric acid, were also examined. The technique of scanning electron microscopy was employed to furnish supplementary information on the nature of these samples.

II. Experimental Procedure

A. Experimental Equipment

1. Electron Beam Microanalyzer

The electron beam microanalyzer (EBMA) is an analytical tool with demonstrated capability for chemical analysis of particulates. Essentially it is a fine focus X-ray tube in which the specimen to be examined becomes the target anode and point by point chemical analysis is performed by the X-ray fluorescent method.

The microanalyzer used for this work was one of three designed and constructed by the Advanced Metals Research Corporation. This instrument is shown in Fig. 1 (a). It is the prototype for the commercially available Philips Electronic Instruments AMR/3 unit. In practice, a beam of electrons is generated at an incandescent tungsten filament and accelerated by means of a high D.C. potential (5-30 KV). The electron beam is focused to a diameter of 1 micron at the specimen surface by means of a system of electromagnetic lenses. As in an X-ray tube, a continuous or white spectrum as well as a characteristic X-ray spectrum are produced. The analysis of the small excited volume in the specimen is afforded by means of a number of X-ray spectrometers designed to examine the available X-ray spectrum.

An optical system (400X magnification) allows continuous visual observation of the area being analyzed. In addition, a system of externally controlled micrometers permits the specimen to be traversed in fixed steps or motor driven beneath the electron beam. The specimen is mounted in a one inch diameter metallurgical mount or fastened to any convenient substrate or holder. One inch diameter Be discs are used for this purpose. Two separate X-ray spectrometers are available for examination of the emitted spectrum. Determination of the wavelength of the characteristic X-rays indicates the elements which are present and a comparison of the intensity of the characteristic X-ray lines to that of a pure element indicates the concentration. Any element from boron through uranium may be analyzed in the present instrument. Scintillation or flow proportional counters are used as detectors. The characteristic lines of low energy are measured in either helium or vacuum.

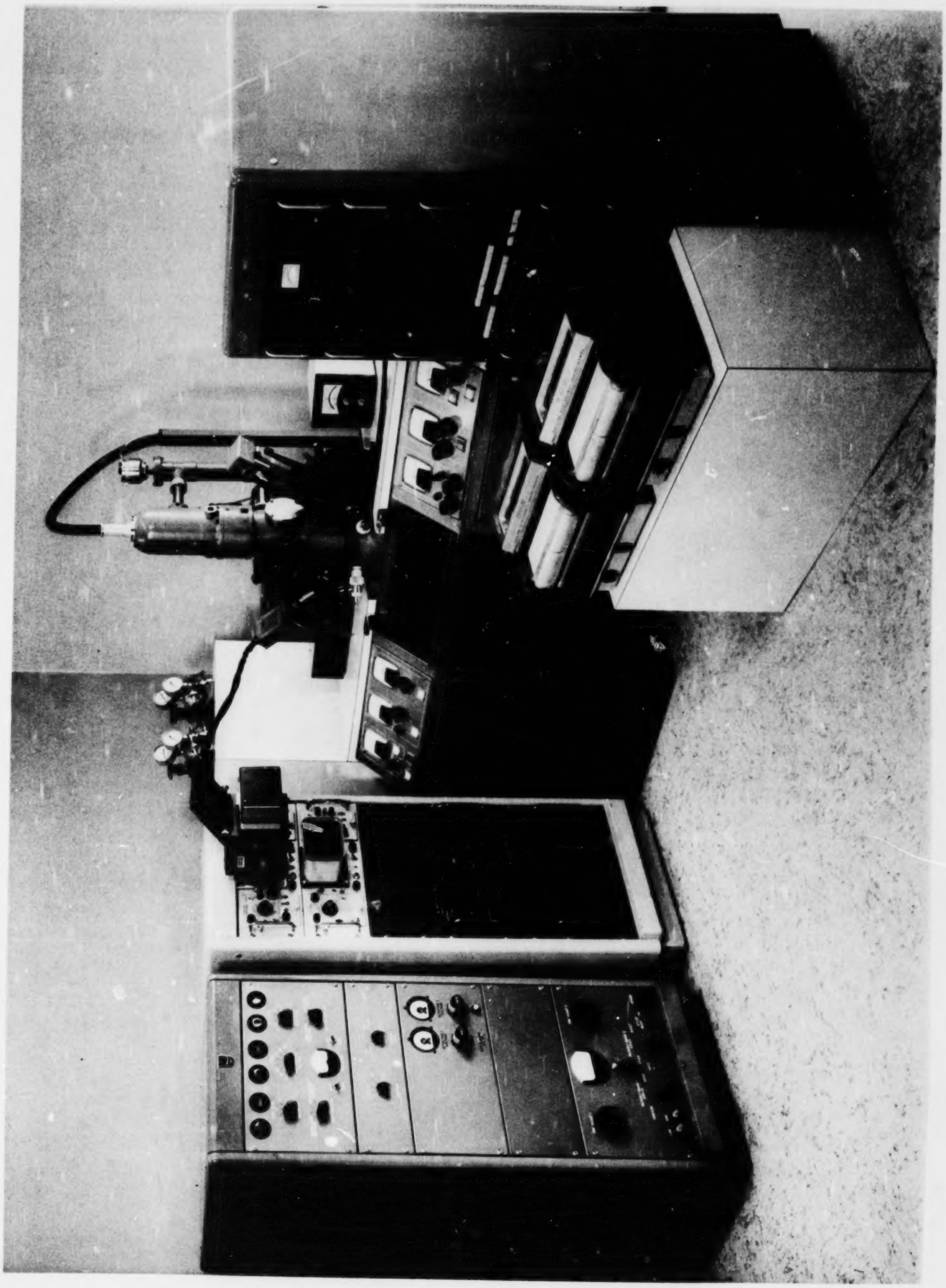

Fig. 1^a The AMR Electron Beam Microanalyzer

The X-rays produced may be collected in a non-dispersive channel. The crystal is bypassed and the X-rays fall directly into the slit of a flow detector. A multi-channel pulse height analyzer may be employed to resolve the spectrum available.

For particle analysis, the microprobe is employed in the following manner. The electron beam is positioned on the particle of interest and a complete spectral pattern is recorded with one of the available spectrometers. Once the general chemistry is known, individual element analysis is performed by aligning the spectrometers to record particular characteristic lines of interest followed by the sequential excitation of the desired particles.

Although the microprobe has sufficient capability to analyze particles which are sub-micron in size, a major drawback in the employment of this technique for small particle analysis lies in the inability to optically resolve the particles which are micron or sub-micron in size.

2. AMR X-ray Spectrometer Attachment for the Electron Microscope

The AMR X-ray Spectrometer Attachment for the Philips EM-200 Electron Microscope provides the microscope with analytical capability similar to that available in the Electron Beam Microanalyzer. Combined with the superior viewing capability available in the Philips EM-200 Electron Microscope, small particle analysis is greatly facilitated. The vacuum spectrometer is equipped with a continuously focusing mica crystal which is capable of analyzing the characteristic X-radiation from any element in the periodic table from Mg through U. Analyses are performed using a flow proportional detector equipped with P-10 gas (90% argon, 10% methane), pulse height analyzer and associated scalar and rate meter circuitry. The X-ray Spectrometer mounted on the objective aperture port on the rotating/tilting stage of the Philips EM-200 Electron Microscope is shown in Fig. 1 (b).

Employing samples typical of those used in conventional microscopy, particulates can be viewed at magnifications up to 100,000X and photographed in the fashion of normal electron microscopy.

Fig. 1 (b)

AMR X-ray Spectrometer Attachment

mounted on Philips EM 200 Electron Microscope

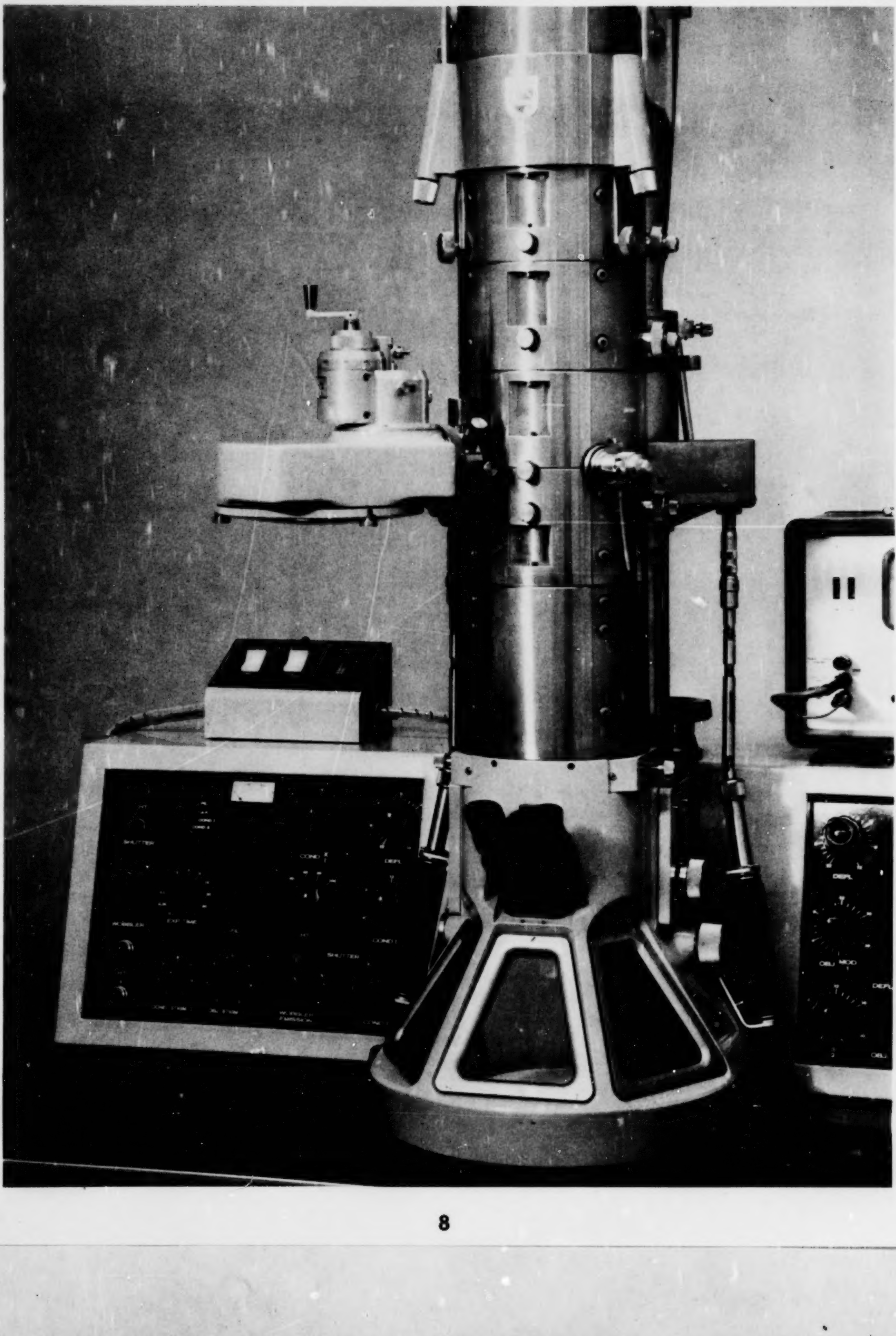
SHUTTER
COND
DEFL
EXP TIME
COND I
SHUTTER
EMISSION
DEFL
OBJ
MOD
DEFL
OBJ

At any instant it is possible to energize the second lens of the double condenser lens system to produce a probe spot down to 1.2 microns in size. X-rays produced in the sample can then be analyzed employing the X-ray spectrometer attachment. By energizing the first condenser lens to control the beam current and the second condenser (or probe forming) lens to control the probe size, the electron beam can be adjusted for maximum current at a given size. (Employing a 500μ first condenser and 700μ second condenser aperture, a minimum spot size of 1.2μ could be realized.) As a result, particles can be continuously viewed during analysis at high magnification. In this way, changes in particle morphology during excitation resulting from volatilization, melting, decomposition, etc. can be monitored and correlated with any observed changes in the characteristic X-ray intensity.

3. Scanning Electron Microscopy

The transmission electron micrographs obtained in the conventional electron microscope are essentially shadowgraphs of the particulate material. Since the Scanning Electron Microscope provides topographical information as well as morphological information, this instrument was employed to furnish supplementary information on the nature of the specimens.

The instrument is electron optically similar to a microbeam analyzer. A beam of electrons is generated from an incandescent tungsten filament and accelerated by means of a high D.C. potential (20 KV). A system of three electromagnetic condenser lenses is used to focus the beam to a diameter of 200A° at the specimen surface. Interaction of the beam with the specimen produces high energy primary back-scattered electrons and low energy (less than 50 eV) secondary electrons. The latter, which are generated from very shallow depths in the sample surface, are collected employing a wire mesh at +300V and accelerated by means of a high D.C. potential (12 KV) towards a plastic scintillator. The scintillator converts the electron beam to light which is then amplified and converted back to an electrical signal by a photomultiplier. This signal is used to modulate the brightness of a cathode ray tube. By sweeping the electron beam in a raster pattern across the specimen in synchronization with the raster in the cathode ray tube, an image of the specimen is produced on the cathode ray screen. This image can be recorded photographically to provide topographical and morphological information about the specimen.

B. Sample Preparation

Samples were supplied by the Division of Chemistry and Physics, National Air Pollution Control Administration, Consumer Protection and Environmental Health Service of the Department of Health, Education and Welfare. The samples which were studied consisted of particulate matter collected from the atmosphere in the vicinity of the city of Los Angeles, California; Auto Exhaust, collected from internal combustion engines burning lead bearing fuel; laboratory generated test aerosols of Na Cl and Zn $(NH_4)_2(SO_4)_2$; and Ni films (~ 1000A° thick) which had been prepared by vacuum evaporation on nitrocellulose substrates supported on standard Cu microscope grids. The latter had been subjected to aerosol droplets of H_2SO_4.

All the particulate collections were sized employing a Battelle Cascade Impactor. For particles of a given mass, each stage of the impactor contains an average particle size which decreases as tabulated in Table I. In general, on a given stage of the impactor, the average size of particles comprised of heavy elements will be smaller than those comprised of lighter elements. As a result, the average sizes listed in Table I can only be considered as approximate.

The specimens which consisted of Ni films had been subjected to aerosol mists, the droplets of which had been sized by employing the Cascade Impactor. These specimens were to be examined to determine the nature of the reaction between the H_2SO_4 droplets and the Ni film.

The particulate specimens were prepared in two ways to facilitate the analysis in the microbeam analyzer and/or the electron microscope. Samples which were to be examined in the microprobe and the scanning electron microscope were collected on one inch beryllium discs which had been metallographically polished through 0.25 micron diamond. Samples which were to be examined in the EM-200 Electron Microscope were collected on carbon coated nitrocellulose substrates which were supported on standard 200 mesh Cu microscope grids. Preliminary analysis of the test aerosols and atmospheric particulates revealed that the particles tended to move when bombarded with electrons, indicating that they were not electrically conducting. In addition, tears

Table 1

Typical Particulate Collections with the Battelle Cascade Impactor

Stage	Average Size (microns)
1	4.0
2	2.0
3	1.0
4	0.50
5	0.25

often developed in the substrate which is believed to have been caused by excessive heating of the particles. As a result, the specimens were coated in a vacuum evaporator with carbon. This coating provided the necessary electrical and thermal conductivity without influencing the X-ray analytical capability. No carbon coating was necessary on the specimens consisting of evaporated Ni on formvar, since they were already conducting.

III. Results and Discussion

A. Optimization of Instrumental Parameters

Since the study of particulate matter in the micron to sub-micron size range requires that such instrumental parameters as beam current, beam size, electron acceleration potential, etc. be optimized, a study of these parameters was undertaken. The intent of this study was to determine the effect on the absolute X-ray intensity (available from particles of a given size) resulting from varying these parameters in a systematic fashion. These investigations will be discussed in subsequent sections in an attempt to correlate these observations with prior knowledge and experience obtained from electron beam microanalysis of semi-infinite specimens.

1. Determination of beam current as a function of beam Size

Since the direct observation of the electron beam diameter is possible in the electron microscope, the determination of the electron beam current as a function of the electron beam size was undertaken. The Philips EM-200 Electron Microscope is equipped with a precision vacuum tube voltmeter/exposure meter (GM6020) for beam current measurements.

The first and second condenser lenses were employed to focus a fine beam of electrons onto the specimen plane. The current setting of the first electromagnetic condenser lens controls the minimum size and current in the electron beam. The second condenser lens is used as a "probe" lens and focuses the beam at the plane of the specimen. A third lens (projector lens) is used to project the focused beam onto a fluorescent screen. By projecting the beam at a magnification of 10,000X, the beam diameter could be measured readily by employing a centimeter scale etched into the fluorescent screen.

The theoretical considerations which govern the design and optimum operation of an electron beam microanalyzer are well established and have been considered in detail elsewhere. Therefore, only a brief review of the considerations involved in the optimization of the electron microscope for microanalysis will be presented. The minimum spot size available in the electron microscope of course is fixed by the geometry of the system. In addition, lens aberrations also increase the ultimate minimum spot size which can be achieved in the instrument. This ultimate spot size d is given as

$$d = dg + 1/2C_s\alpha^3 = Mdo + 1/2C_s\alpha^3 \quad (1)$$

Where M is the magnification of the two lens system, do is the size of the source, Cs is the spherical aberration coefficient, and α is the half angle subtended from the image by the lens aperture. This equation does not account for the additional aberrations of astigmatism and chromatic aberration. These aberrations are not large and will therefore not be considered. Although in theory the beam size can be reduced to any diameter by decreasing the magnification (increasing the demagnification) and also the angular aperture, α, there is a concurrent large reduction in probe intensity which imposes a practical limitation on the minimum beam size. The maximum current available in an electron beam of diameter, d, is given by

$$i = \frac{9}{64} \frac{eV}{KT} io \frac{d^{8/3}}{(2C_s)^{2/3}} \quad (2)$$

where io = the current in the source.

To obtain this maximum current, the aperture half angle α is given by

$$\alpha = \left(\frac{d}{2C_s}\right)^{1/3} \quad (3)$$

From these considerations, the following steps were taken to optimize the electron microscope for electron beam microanalysis.

To insure maximum current in the probe spot, the electron gun was operated close to optimum emission. This was accomplished by adjusting the gun cathode cap (Wehnelt cylinder) of the standard EM-200 electron gun with respect to the filament position to obtain electron currents approaching the maximum allowable emission for the acceleration potential in use. The maximum allowable emission as a function of accelerating potential is listed in Table 2.

Table 2

Maximum Allowable Emission for Philips EM-200 Electron Gun

Emission Current (μ amps)	KV
92	40
108	60
124	80
140	100

To insure maximum current in the final probe spot, the following criteria were employed. The maximization of current in a beam of diameter, d, requires the employment of an aperture such that α is given by equation (3). Since it is not feasible to change apertures every time one wishes to employ a different beam size, the following criterion was adopted. The aperture system was adjusted to give an optimum beam current at the limiting spot size of approximately 1.2 microns. This beam diameter could be reduced to a size which was less than 1 micron (0.8 - 0.9 microns), but not without a considerable reduction in beam current. The aperture system which was employed consisted of a 700μ diameter second condenser aperture and a 500μ first condenser aperture. A measure of the current in the beam as a function of spot size was obtained employing the Philips vacuum tube voltmeter/exposure meter GM6020 provided with the EM-200 Electron Microscope. With no specimen in place, the beam was projected and focused at 10,000X on the final viewing screen. The beam current (reduced by a constant fraction of backscattered electrons) was read directly from the meter. Simultaneously, the size of the spot was measured directly on the screen. Fig. 2 shows the results of the study conducted at 60 KV, employing gun emission of 90 microamperes. As mentioned previously, the limiting beam size was found to be in the vicinity of 1.2 microns.

2. Effect of Increasing Electron Acceleration Potential

Since the characteristic X-ray intensity available is dependent on the energy of the electrons which give rise to them, increasing the acceleration potential of the electrons has a direct effect on the X-ray intensity. Characteristic lines are not excited unless the voltage exceeds the critical value Vo, necessary to remove an electron entirely from an atom in the target. The intensity, I, of the characteristic line increases with voltage V, and beam current i approximately according to the relation

$$I = Ci\,(V-Vo)^{n} \qquad (4)$$

where C is a proportionality constant and Vo is the excitation voltage. The exponent n is slightly less than 2 if V is less than two to three times Vo and approaches unity at higher voltages. Equation (4), of course, is applicable only when the material being bombarded is semi-infinite in extent, i.e. only

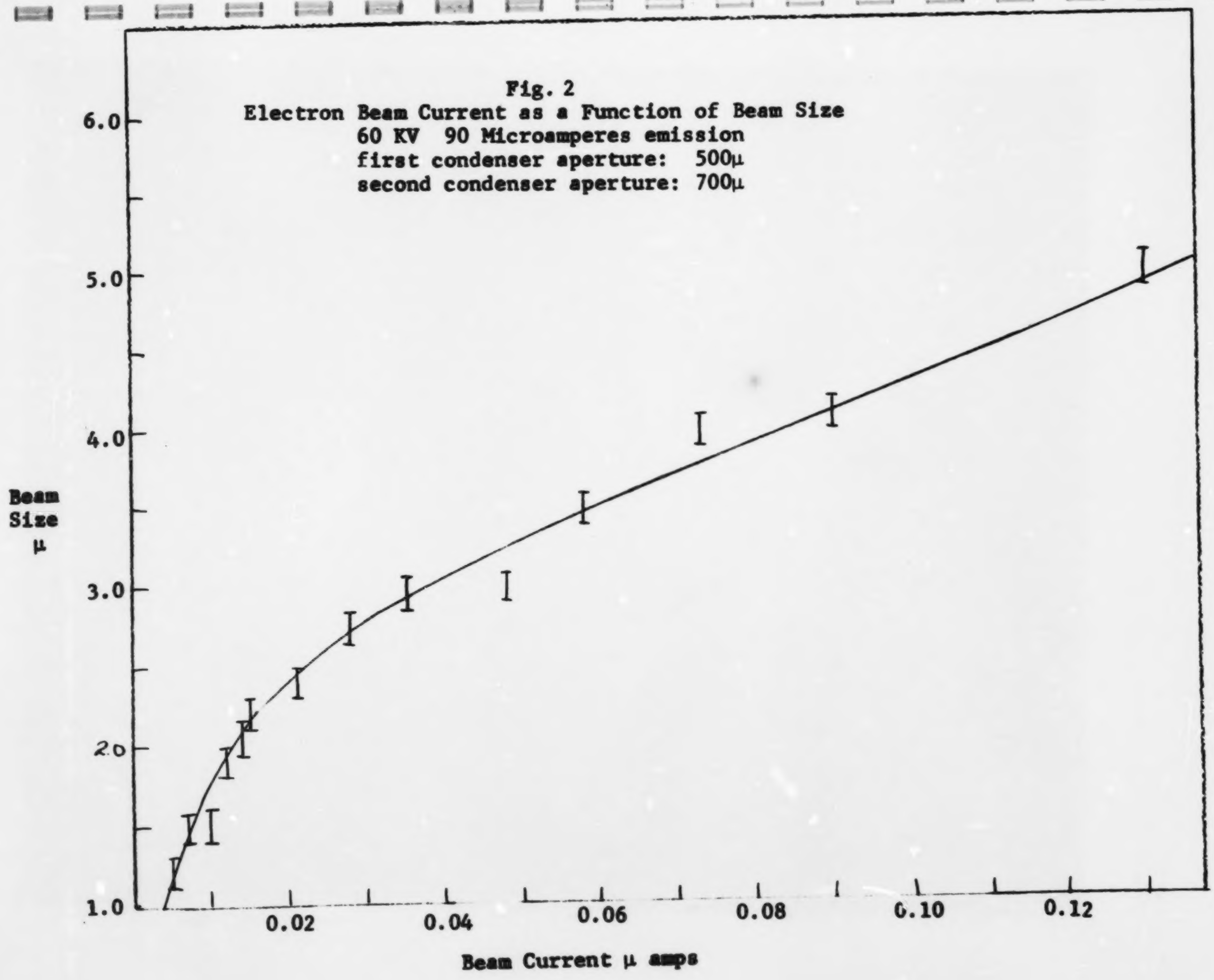

Fig. 2
Electron Beam Current as a Function of Beam Size
60 KV 90 Microamperes emission
first condenser aperture: 500µ
second condenser aperture: 700µ

when the beam does not penetrate the sample.

From these considerations, increasing the acceleration potential in the electron microscope results in an increase in the X-ray intensity according to equation (4), but this increase is partially compensated by the fact that fewer of the electrons are absorbed by the finite sample (due to their higher energy).

Finally, another factor which has the effect of increasing the X-ray intensity as the acceleration potential is increased must be considered. The maximum allowable emission available from the electron gun increases with voltage, more beam current is available at higher potentials. Since in normal operation a fixed bias on the electron gun (fixed filament to anode cap spacing) is used, the emission current and hence the final beam current increases with increasing electron acceleration potential. This increase in beam current was measured and is listed in Table 3. For this investigation the anode cap was fixed to provide an emission of 90μ amps at 60 KV.

3. Conversion of X-ray Intensity to Concentration

In general, the microprobe analysis requires the conversion of X-ray intensity to chemical concentration. These conversion procedures are well established for semi-infinite specimens, and can be separated into three principle correction terms: Absorption path correction, Fluorescence correction, and Atomic Number Correction. It is not possible to generalize the relative influence of these corrections as a function of particle size, since they depend greatly upon the wave length of the characteristic X-rays being measured as well as the absorption of these X-rays by the other elements in the particle. At best, one can only describe the procedures one would employ to assess the magnitude of these corrections.

For particles larger than 5-10 microns in diameter, the classical procedures which correct for these effects are generally applicable. For particles less than 0.5 microns in size these effects are generally negligible. For the size range 0.5 microns to 5 microns, quantitative chemical calculations will, in general, have to be based on the use of standard mineral or element calibration methods. For particles which contain a number of elements, the relative changes in X-ray intensity as

Table 3

Beam Current as a Function of Electron Acceleration Potential

Emission: 90μ amps at 60KV

KV	Beam Current microamps	Beam Diameter microns
40	0.056	5
60	0.11	4.5 - 5
80	0.21	4.5 - 5

a function of particle size should prove to be one of the best tests for determining whether correction procedures need to be applied. For example, if absorption effects are not negligible, the relative X-ray intensity of one element in the particle with respect to another element should change as the particle size increases from 0.5 to 5 microns. This analytical approach requires the measurement of the characteristic X-ray lines from at least two different elements in the particle. Comparisons with the infinite particle (≥ 5 microns) or with the extremely small particle (0.5μ) should indicate the magnitude of the corrections.

The X-ray take off angle is another important instrument parameter which influences the length of the absorption path. For most instruments, the angle between the incident electron beam and the X-ray path to the spectrometer is fixed. For semi-infinite specimens the effect of take off angle can be measured by rotating the sample with respect to the incident electron beam and the X-ray path. This procedure cannot be employed for particulates, since it in effect does not change the length of the absorption path but merely rotates the particle. As a result, the effect of changing the X-ray take off angle can not be investigated.

4. Summary of Instrument Optimization in Relation to Small Particle Analysis

As described above, the optimization of the electron microscope for small particle analysis is accomplished by maximizing the emission of the electron gun to provide the brightest possible electron source, and optimizing the aperture system to provide an electron beam with enough current to perform small particle analysis. Since these parameters, in effect, result in maximizing the brightness of the incident electron beam, they can be optimized without considering the type of sample which is to be analyzed. The latter is not true for optimization of the electron acceleration potential or the size of the electron beam. The former has already been discussed qualitatively for the analysis of finite specimens, e.g. particulates. The optimum beam size depends largely on the nature of the specimen to be analyzed. Qualitatively, optimization of the beam diameter depends on the following considerations. In this discussion, the optimum beam size is defined as that beam size which results in the maximum X-ray intensity available from particles of a given size. In effect, this definition means that the electron beam size employed for analysis could conceivably be larger than the particle size, provided the particles were dispersed sufficiently for the necessary area resolution.

First, consider the analysis of a particle which is infinitely large with respect to the electron beam. For a given acceleration potential, the X-ray intensity available from this particle would depend only on the electron current in the beam. Since, for the most part, the particles to be analyzed are finite with respect to the beam, the X-ray intensity available from the particle depends on the electron current in the area subtended by the particle. In general, the current per unit area (current density) in the electron beam decreases with decreasing spot size. As a result, employing a beam larger than the specimen could result in higher X-ray intensity, provided the increased electron current density compensated for the fact that the particle would subtend a smaller fraction of the beam.

In addition to the effect of current density, one must also consider the effect of the distribution of electrons in the beam. This distribution is not uniform, but rather increases from the outer edge to the center in a gaussian fashion. This increased electron density close to the center of the beam indicates that measurement of the beam size and the total beam current is not sufficient to establish the electron current subtended by a particle which is smaller than the electron beam.

From the above discussion, one can see that systematic investigation of the influence of electron acceleration potential, electron beam current and diameter on the X-ray intensity available from particles which vary in size would contribute important information in the general field of small particle analysis. In the next section, the results of this type of investigation on laboratory test aerosols are described.

B. Studies of Laboratory Test Aerosols

The laboratory test aerosol samples which were examined were sized and carbon coated in the manner described previously. The particles were mounted on nitrocellulose substrates supported on standard Cu microscope grids.

1. Sodium Chloride

The test aerosols of Na Cl available from the different stages of the Battelle Impactor were found to cover a size range from 3 microns to 0.25 microns. The particles were observed to be predominately cubic in shape. Attempts to analyze these specimens proved to be unsuccessful, due to the visible decomposition of the particles under electron beam bombardment. Employing a one micron beam (0.01 microamperes beam current) at 80 KV to analyze a one micron particle, the particle did not decompose and the Cl Kα (1) X-ray line was found to be approximately 50 counts per second. However, when larger beam sizes (and higher beam currents) were employed or smaller particles were examined decomposition occurred. For the one micron particle, decomposition was evident at a beam diameter of 1.5 microns (0.02 microamperes beam current). As a result, for the Na Cl test aerosol it was not possible to ascertain the effect of electron acceleration potential, beam size (and current) on the production of characteristic X-rays in particles of varying size.

2. Zinc Ammonium Sulfate

The $Zn(NH_3)_2\ (SO_4)_2$ test aerosols proved to be much more satisfactory for these studies. No visible decomposition could be observed at 10,000X in the electron microscope. To further determine whether any decomposition occurred, the ZnKα and SKα X-ray intensities were employed. The beam was positioned on the particles and the X-ray intensity was recorded as a function of time. No change in the ZnKα intensity was observed. However, the SKα was found to drop rapidly initially and then stabilize at a much lower level, indicating S is lost from the particle during electron beam bombardment. The fact that the ZnKα intensity was stable indicated that this element, at least, could be employed to perform the desired study. Consequently, particles of zinc ammonium sulfate ($Zn(NH_4)_2\ (SO_4)_2$) ranging from 3 microns to 0.25 microns in diameter were employed to determine the effect of beam size and acceleration potential on the ZnKα X-ray intensity. Since the SKα intensity could not be measured, it was not possible to determine the magnitude of the absorption, fluorescence and atomic number corrections as a function of particle size (see section III_3). The particle morphology was predominately spherical.

The result of the investigation for a 3 micron and 2 micron particle are listed in Tables 4 and 5 respectively. Table 6 summarizes the variation of X-ray intensity with beam size at 80 KV for particle diameters ranging from 0.4 microns to 1 micron. No measurable X-ray intensity was available from particles 0.25 microns in diameter.

It should be noted that the beam diameters were measured at 10,000X on the fluorescent screen of the electron microscope and are subject to errors as large as ± 10%. Since the beam was focused to minimum diameter, a better measure of equivalent beam size at any given acceleration potential is obtained by employing the criterion of equivalent beam current.

a. Current Density vs Beam Size

From these results, the electron current per unit area of beam current was determined and is listed in Table 7. Although much scatter exists in the data due to the uncertainty in the beam diameter, the current density is found to increase rapidly with beam size initially, after which it levels off or may even exhibit a maximum at lower acceleration potential. Since the aperture angle has only been optimized for one beam size (1.2 microns), the current density does not increase with spot size as rapidly as it would if the aperture angle, α, were optimized for all beam sizes. Increasing the gun potential has a strong effect on increasing the current density. Each 20 KV incremental increase results in a current density increase of 1.5 to 2 times. This increase is due to the higher gun emission at higher KV. It should be remembered that the maximum allowable emission increases with increasing gun potential.

b. X-ray Intensity vs Acceleration Potential

Although higher electron acceleration potentials result in an increase in the beam current, the increase in beam energy must also be considered. The latter results in less sample absorption and, therefore, less X-ray yield per electron. The magnitude of this effect is shown in Tables 8 and 9 for a 3 micron and 2 micron diameter particle, respectively and in Table 10 for micron and sub-micron particles.

The X-ray yield (counts per second/microampere) is reduced with increasing potential. However, the increased beam

Table 4

Effect of Beam Size and Acceleration Potential on Zn Kα X-ray Intensity from a 3μ Particle of $Zn(NH_4)_2(SO_4)_2$

Beam Dia. (Microns)	Beam Current (Microamperes)			X-ray Intensity (counts/sec.)		
	80KV	60KV	40KV	80KV	60KV	40KV
6.5	0.30	0.17	-	148	102	-
6	-	-	0.06	-	-	43
5	0.192	0.114	-	122	82	-
4.5	-	-	0.035	-	-	30
4	0.114	0.065	-	70	52	-
3.5	0.092	-	-	50	-	-
3.2	0.078	0.046	-	36	30	-
3.0	-	-	0.023	-	-	20
2.8	0.060	-	-	31	-	-
2.5	-	0.025	0.015	-	16	11
2.2	0.034	-	-	15	-	-
2.0	-	0.017	0.008	-	8	4
1.6	0.016	-	-	6	-	-

Table 5

Effect of Beam Size and Acceleration Potential on ZnKα X-ray Intensity from a 2μ Particle of $Zn(NH_4)_2(SO_4)_2$

Beam Dia. (Microns)	Beam Current (Microamperes)		X-ray Intensity (counts/sec.)	
	80KV	60KV	80KV	60KV
6.5	0.38	-	72	-
5.3	0.23	-	59	-
5.0	-	0.14	-	40
4.0	0.135	0.084	56	36
3.5	0.086	-	47	-
3	0.051	0.042	34	27
2.5	-	0.018	-	13
1.8-2.0	0.022	0.012	15	9
1.5-1.6	0.007	0.0045	5.5	4

Table 6

ZnKα Intensity Versus Beam Diameter at 80KV for Sub-Micron Particles of $Zn(NH_3)_2(SO_4)_2$

Beam Dia. (Microns)	Beam Current (Microamperes)			X-ray Intensity (counts per second)		
	1μ	0.6μ	0.4μ	1μ	0.6μ	0.4μ
6μ	0.29	-	0.29	15	-	4
5.5	-	0.26	-	-	9	-
5	-	0.17	0.19	-	18	10
4.5	0.16	-	0.16	23	-	11
4	-	0.10	0.14	-	28	8
3	0.075	0.065	0.083	25	20	5
2.5	0.043	-	-	18	-	-
2	0.021	0.025	-	11	10	-
1.5	0.008	0.007	-	4.5	3	-

Table 7

Current Density as a Function of Acceleration Potential

D Beam Diameter (microns)	Current Density i/D^2 (microamps/micron^2)		
	80KV	60KV	40KV
6.5	0.00805	0.00402	-
6.0	0.00805	-	0.00167
5.0	0.0077	0.00508	-
4.5	0.0079	-	0.00173
4.0	0.0077	0.00468	-
3.0	0.0076	0.00460	0.00258
2.5	0.00688	0.00352	0.00240
2.0	0.00575	0.00425	0.0020
1.5	0.003	0.00200	-

Table 8

ZnKα X-ray Intensity Per Microampere of Beam Current from a 3μ Particle of $Zn(NH_3)_2(SO_4)_2$

D (Microns)	I/i (counts/sec. per Microampere)		
	80KV	60KV	40KV
6.5	4940	5990	-
6	-	-	7170
5	6350	7200	-
4.5	-	-	8570
4	6140	8000	-
3.5	5440	-	-
3.2	4620	6530	-
3.0	-	-	8700
2.8	5160	-	-
2.5	-	6400	7340
2.2	4420	-	-
2.0	-	4700	5000
1.6	3740	-	-

Table 9

ZnKα X-ray Intensity per Microampere of Beam Current from a 2μ Particle of $Zn(NH_3)_2(SO_4)_2$

D (microns)	I/i (counts/sec. per microampere)	
	80KV	60KV
6.5	189	-
5.3	258	-
5	-	286
4	415	429
3.5	546	-
3	666	642
2.5	-	722
1.8-2.0	684	750
1.5-1.6	786	1125

Table 10

ZnKα X-ray Intensity per Microampere of Beam Current at 80KV from Sub-Micron Particles of $Zn(NH_3)_2(SO_4)_2$

Beam Dia. (Microns)	I/i (counts per second/μ amp)		
	1μ	0.6μ	0.4μ
6	51.7	-	13.8
5.5	-	34.6	-
5	-	106	52.7
4.5	144	-	68.6
4	-	280	57.1
3	334	308	60.2
2.5	419	-	-
2	524	400	-
1.5	563	429	-

current results in a net increase in X-ray intensity as shown in Tables 4 and 5. Since in the analysis of small particles one is primarily concerned with obtaining maximum sensitivity, these results indicate that the gun potential should be maximized.

c. X-ray Intensity vs Beam Diameter

Since the X-ray intensity available from a particle is dependent on the number of electrons impinging on it, the X-ray intensity should be directly related to the current density. It should be noted that the value of current density expressed as total beam current per unit area does not take into account the fact that the distribution of electrons in the beam is not uniform. As a result, an exact correlation between X-ray intensity and current density should not be expected. Nevertheless, the X-ray intensity does in general increase with increasing current density (see tables 4, 5, 6 and 7). As previously discussed one observes that the beam diameter does not have to be equal to or smaller than the particle diameter for maximum sensitivity. As long as the particles are sufficiently well separated, larger beam diameters can be employed. For particles one micron or smaller in size, a maximum in X-ray intensity was observed corresponding to a beam diameter between 3 and 5 microns (See Table 6), which strongly suggests that a maximum in the number of electrons bathing the particle exists. This maximum is not observed in the larger particles since they intercept a larger fraction of the beam (see Tables 4 and 5). These results indicate that when area resolution is not a requirement, small particles should be analyzed with beams ranging in size up to several microns. The actual beam size employed should be investigated to determine the existence of a maximum.

d. Summary

Employing the results obtained in this study, a number of specimens were analyzed in the electron microscope under optimum conditions. In general, the X-ray intensity was maximized by employing an 80 KV acceleration potential and a 3 to 5μ beam size. The results obtained from these studies are described in the following sections.

C. Atmospheric Samples

1. Electron Beam Microanalysis

Atmospheric aerosol particles, mounted on the polished Be substrates, which had been collected in the vicinity of Los Angeles, California were studied in the Electron Beam Microanalyzer.

Since the ability to analyze particles in the Microanalyzer is limited by the light optical system, only stages three and five were examined. A more extensive study, performed in the electron microscope, is reported in the next section.

Stage five consisted of a very fine, densely packed particulate dispersion. Stained areas were also observed which appeared to have resulted from contact with moisture or acid and possible reaction with the Be substrate. Stage three consisted of coarser and more widely separated particles. Since individual particles could be differentiated in Sample 3 and not in Sample 5, an average analysis was performed on the latter while individual particles were analyzed in the former.

The following remarks summarize the results of this examination. The particles from Stage 3 were found to consist predominantly of Ca, Si, and Fe. Some particles also indicated traces of Mg and Ti. The presence of Fe is subject to question since the Be substrate was found to contain Fe-rich and Si-rich impurities. However, the Fe content (in most of the Fe bearing particles) and Si (in all of the Si bearing particles) was higher than the average concentration of these elements in the substrate. Table II summarizes the intensities of the important characteristic x-ray lines of the elements found in these particles. These intensities are reported in counts per second after subtracting background, and the background intensity is also indicated as well as the x-ray lines observed from impurities in the Be substrate. The specimen current measured during the analysis was of the order of 0.2 microamperes. From these results, it is clear that many of the particles observed on Stage 3 are different chemical compounds. It is probable that these particles are predominately silicates rich in Ca, and/or Fe. The presence of Al, Mg, and Ti compounds and Ca compounds (e.g. CaO or $CaCO_3$) is also indicated.

The analysis of the densely packed particulate matter in Stage 5 revealed that it was composed predominately of the light

Table 11

Summary of Electron Beam Microanalysis of Particles on Stage 3

Acceleration Potential: 30KV

Specimen Current: 0.2 Microamperes

X-ray intensity (counts/sec)

Area	CaKα(3)	CaKα(2)	FeKα(3)	SiKα(1)	AlKα(1)	TiKα(1)	MgKα(1)	Bkgnd
Be Substrate	-	-	80	-	-	-	-	85
Particle 1	-	-	240	60	-	-	-	85
Particle 2	300	85	-	175	30	-	-	80
Particle 3	80	n.d.	190	110	-	-	-	70
Particle 4	30	n.d.	90	-	-	-	-	65
Particle 5	80	n.d.	130	-	-	300	20	70
Particle 6	250	70	200	210	80	-	-	80
Particle 7	135	-	255	310	-	-	-	90
Particle 8	15	n.d.	170	45	-	-	-	80

n.d. = not detected

elements, S, C, and O with traces of Fe and Si. The positive identification of the latter two elements are subject to some question for the same reasons discussed previously. However, these elements were found to be somewhat higher than the average concentration associated with the Be substrate and in addition, were more uniformly distributed. Typical average Fe and Si were in the vicinity of 40 and 20 counts per second respectively compared to background of 20 and 10 counts per second from the Be substrate. As described in a later section, the Scanning Electron Microscopy confirmed the presence of organic matter on this stage.

2. Electron Microscopy/Electron Beam Microanalysis

The atmospheric aerosol particles collected on electron microscope grids were extensively analyzed in the electron microscope. Particles from all of the stages (2 through 5) were surveyed. Samples from stage 2 were chosen for initial examination. Observation of particulate matter on this stage revealed the presence of particles which were extremely spherical in shape. These particles were found to be quite rich in Si, with major amounts of Al and Fe. Si and Fe were elements which had been found in the microprobe examination of stage 3 samples (mounted on polished Be). As previously reported, attempts to analyze these particles without an evaporated carbon coating were unsuccessful since they were observed to move under bombardment of the beam. In addition, the nitro-cellulose supporting film was observed to rupture. Since carbon coating eliminated these effects, the particles were believed to have been charging up and heating during bombardment, indicating that they are poor thermal and electrical conductors. As a result, they are more than likely iron aluminum silicates.

To corroborate the results obtained from the study of $Zn(NH_4)_2(SO_4)_2$ test aerosols, the effect of varying beam size on the SiKα x-ray intensity was examined for a 2 micron and 1 micron particle, respectively. This study was performed at 60 KV, employing an emission current of 90 microamperes. The results, listed in Tables 12 and 13, respectively, generally support the previous conclusions.

To summarize, the x-ray intensity was highest for electron beams which overbathed the particles. The x-ray intensity available from the particles was dependent on the current in the area subtended by the particle. As a result, when current density in the beam (i/D^2) decreased, the x-ray intensity also

Table 12

Si Kα X-ray Intensity vs. Beam Size for a 2μ Diameter Los Angeles Smog Particle

60KV, 90 microamperes emission

D Beam Size	i Beam Current (μ amps)	I SiKα (Cps)	I/i	I/D^2
μ	0.12	235	1960	0.0048
4μ	0.07	180	2500	0.0043
3μ	0.032	125	3900	0.0035
2μ	0.01	50	5000	0.0025

Table 13

SiKα X-ray Intensity vs. Beam Size for a 1μ Diameter Los Angeles Smog Particle

60KV, 90 microamperes emission

Beam Size	Beam Current (μ amps)	I SiKα (cps)	I/i
5μ	0.11	33	300
4μ	0.075	30	400
3μ	0.038	20	526
2μ	0.013	15	1150

decreased. For example, employing a 2 micron and a 5 micron beam, respectively, to analyze the 2 micron particle, the current per unit area was found to increase by a factor of 2 as the beam size was increased, and the x-ray intensity was found to increase by a factor of 4 to 5 (see Table 10).

In addition to these results, spectral patterns were obtained from the 2 micron sphere by employing beam diameters ranging from 2 to 5 microns. These results, which are shown in Figs. 3 through 6, dramatically illustrate the improved analytical capability at the larger beam sizes. The patterns show the major elements present in the particles (Si, Al, and Fe). There is also a strong indication of the presence of Cu which arises from the fact that electrons which are scattered from the particle and the carbon coated nitrocellulose substrate are capable of reaching the supporting Cu grid and have sufficient energy to produce the characteristic K lines of Cu. This "background" is reduced as the size of the beam is reduced, but not without a corresponding loss of the characteristic x-ray intensity available from the particle. Since the Cu spectrum is completely resolved from the particle spectrum, no interference difficulties are experienced by employing larger beam diameters.

Fig. 7 through 26 are spectral patterns obtained from randomly selected particles from all the stages of the collection. Superimposed on many of these patterns are photo micrographs obtained from the particles during analysis in the electron microscope.

The size of particles was found to vary considerably on the microscope grids comprising the second stage of the collection. Particle sizes were found to range from four to five microns to one micron. As would be expected, the number of particles accumulated on this stage was found to be greater than on subsequent stages. Figs. 7 through 16 are the spectral patterns obtained from the second stage of the collection. As can be seen from these patterns, adequate x-ray intensity was available to identify the major chemical species found in the particles. In addition to the spherically shaped particles which were believed to be iron aluminum silicates, a number of calcium rich particles were found. Not all of the latter were of the same chemical species. For example, those represented in Figs. 10 and 11 were found to be rich in Fe, Mg, Ti and Si as well as in Ca, while those in Figs. 7, 8 and 9 were found to be rich only in Ca. In addition to the elements found in these particles, other major

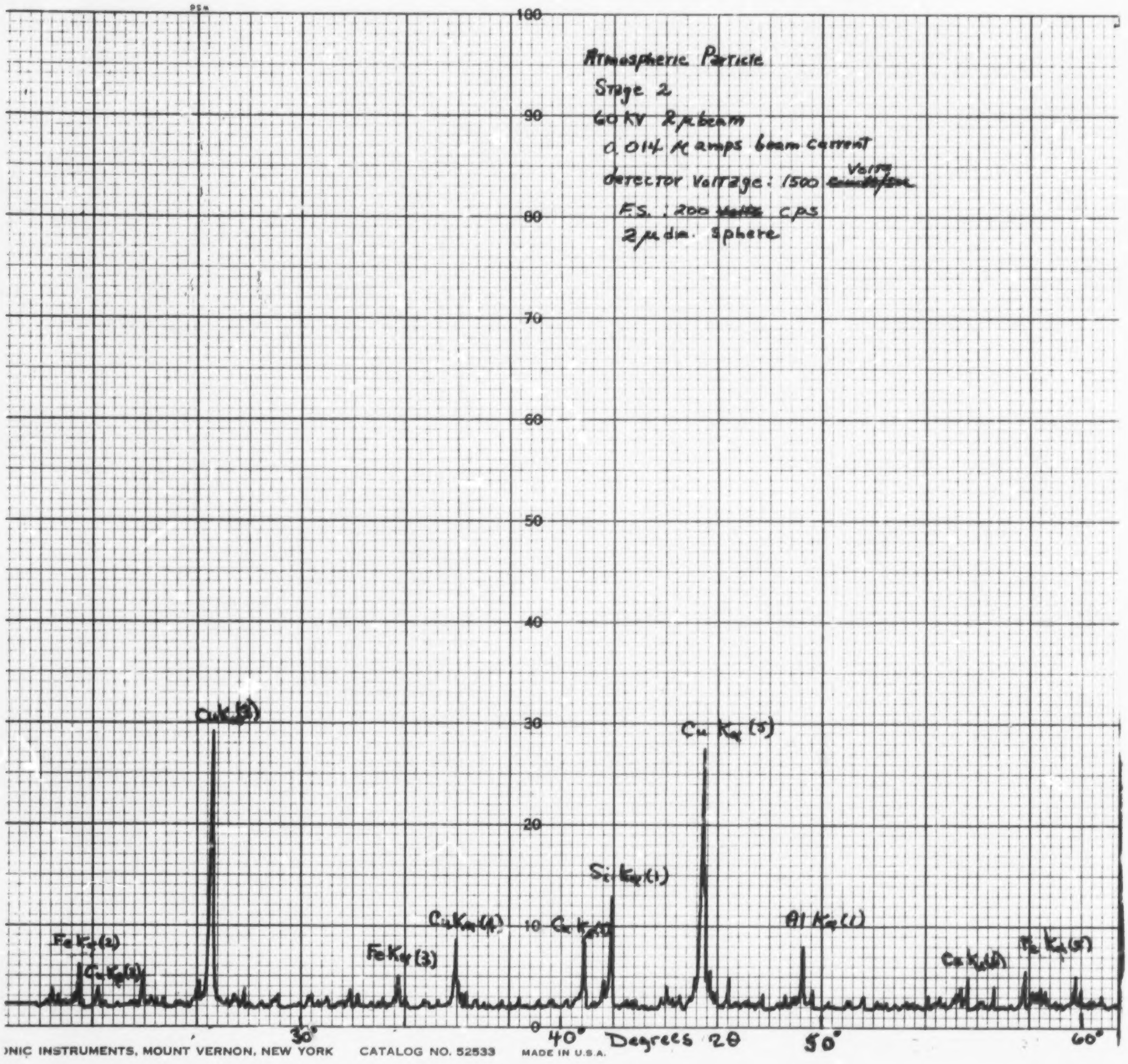

Fig. 3 Spectral Pattern from 2μ Dia. Fe Al Silicate Particle
Employing a 2μ Dia. Beam

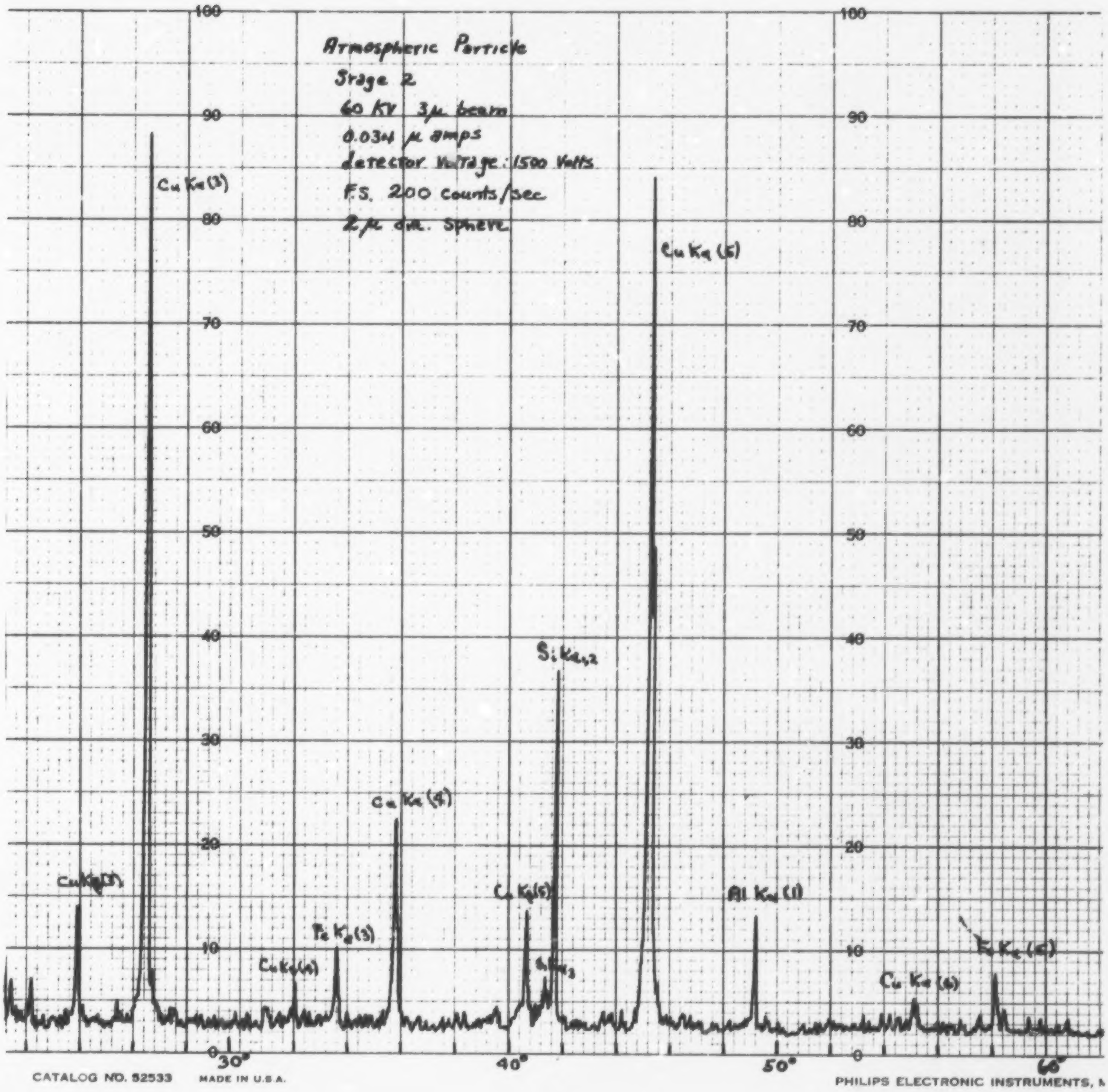

Fig. 4 Spectral Pattern from 2μ Dia. Fe Al Silicate Particle Employing a 3μ Dia. Beam

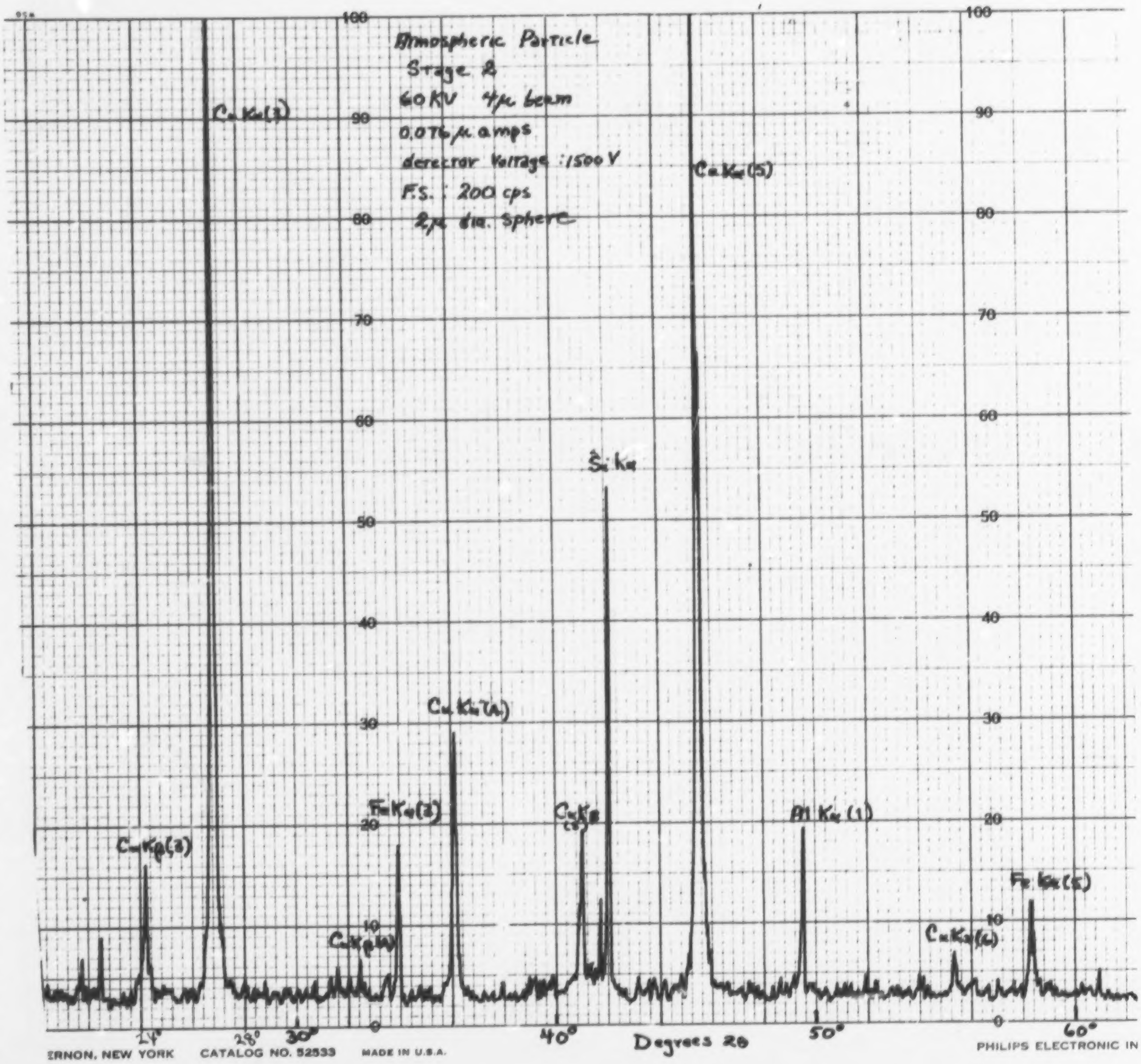

Fig. 5 Spectral Pattern from a 2μ Dia. Fe Al Silicate Particle Employing a 4μ Dia. Beam

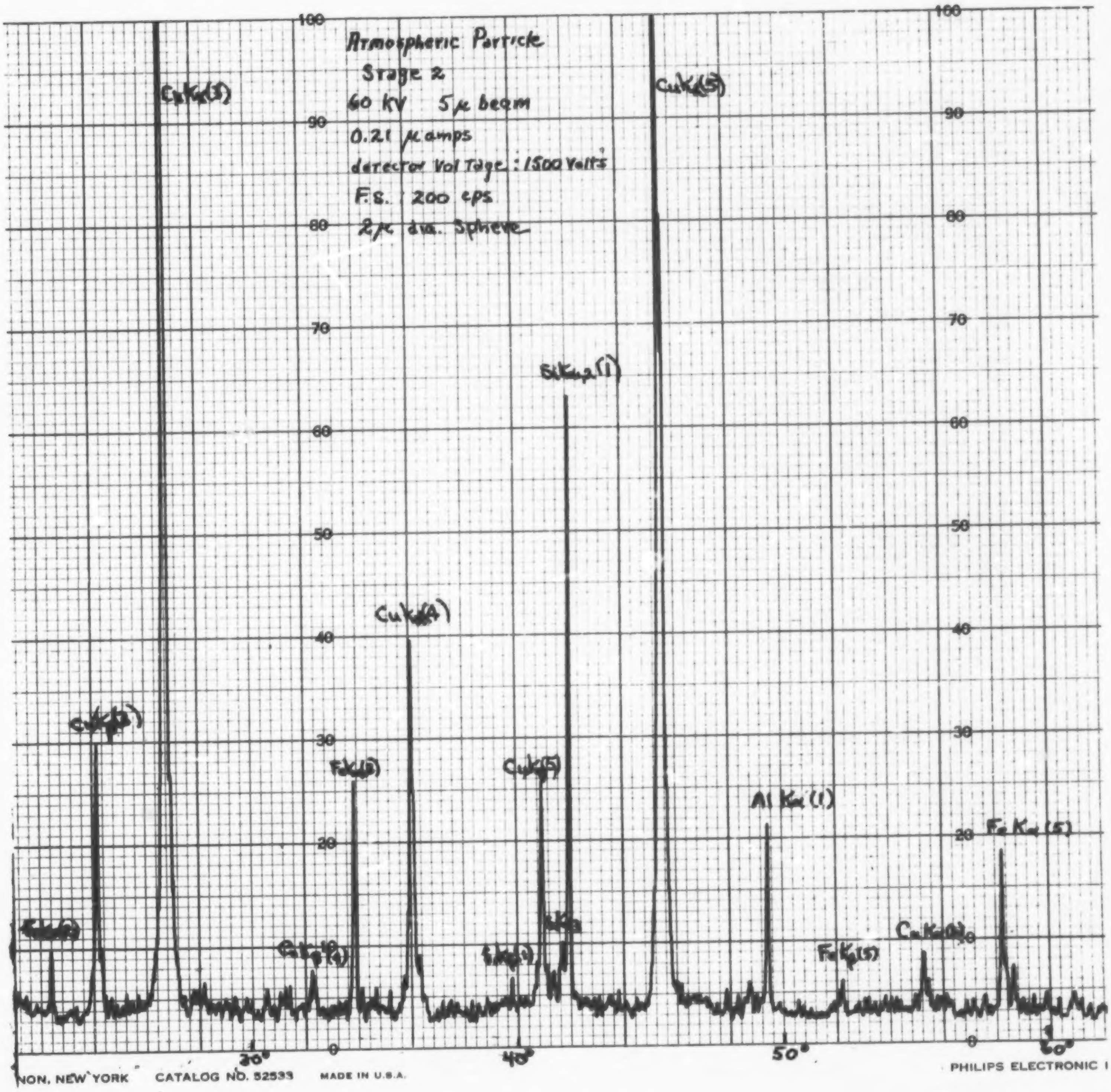

Fig. 6 Spectral Pattern from a 2μ Dia. Fe Al Silicate Particle Employing a 5μ Dia. Beam

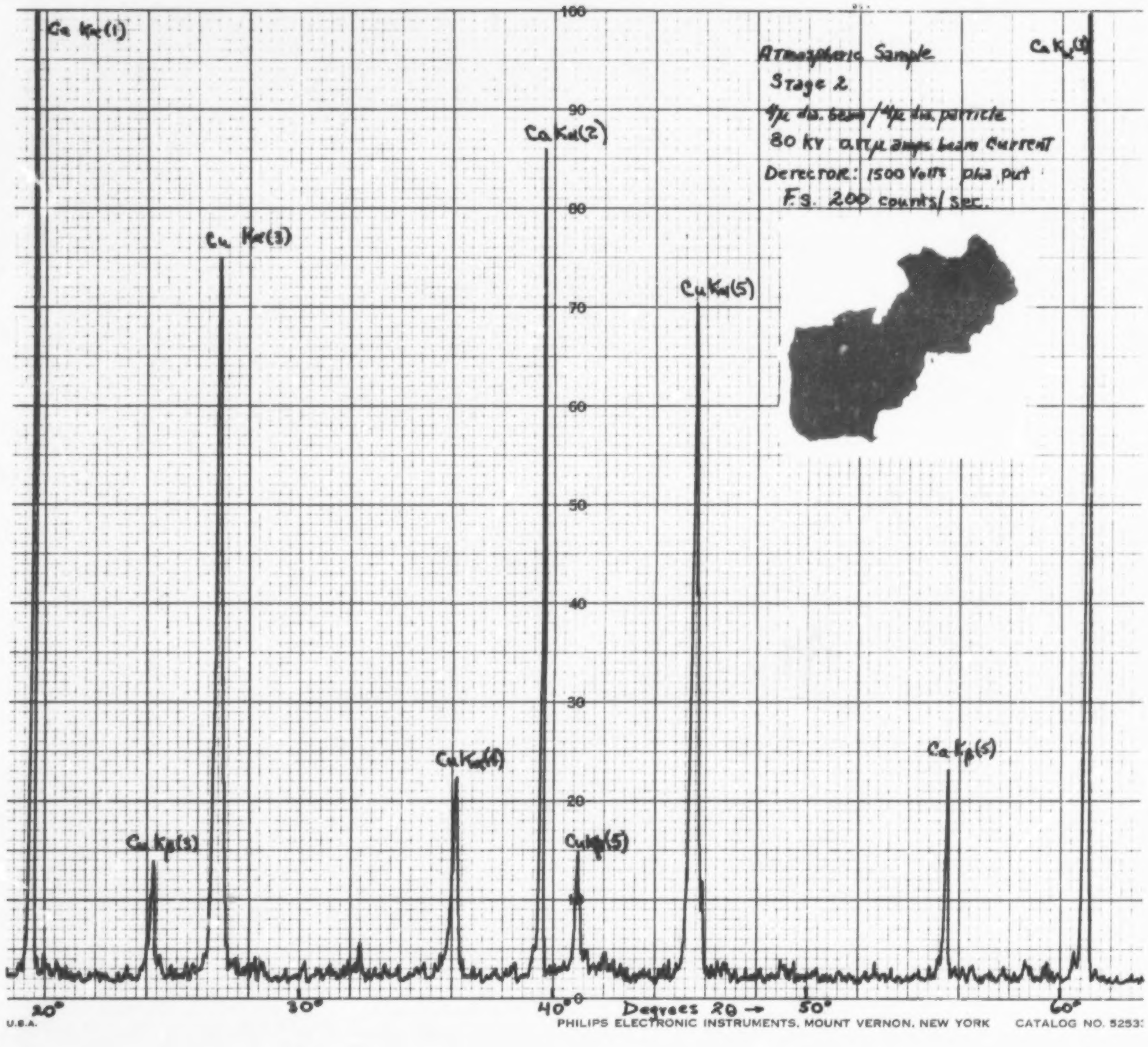

Fig. 7 Spectral Pattern from a 4μ Ca rich Particle

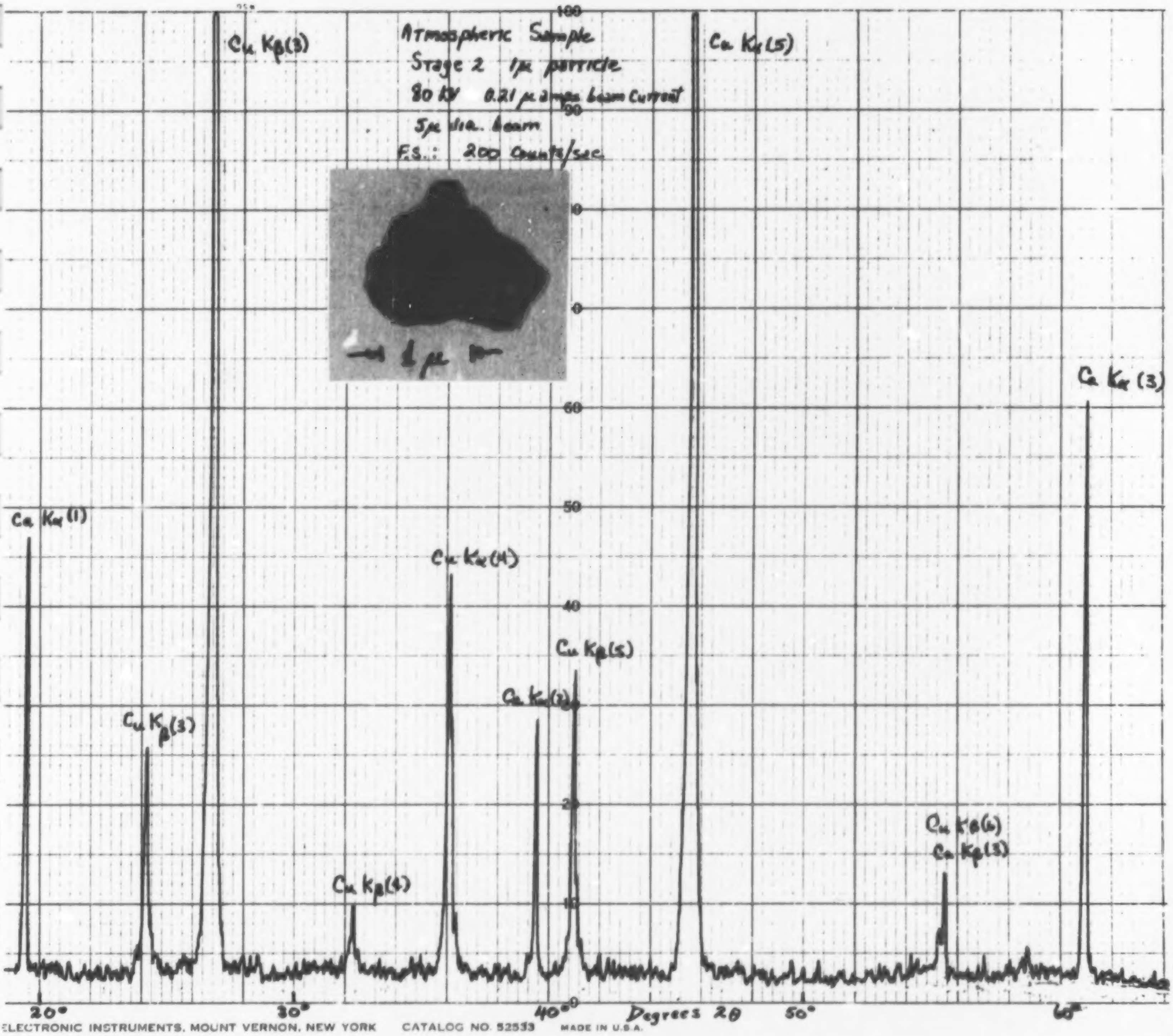

Fig. 8 Spectral Pattern from a 1μ Ca rich Particle

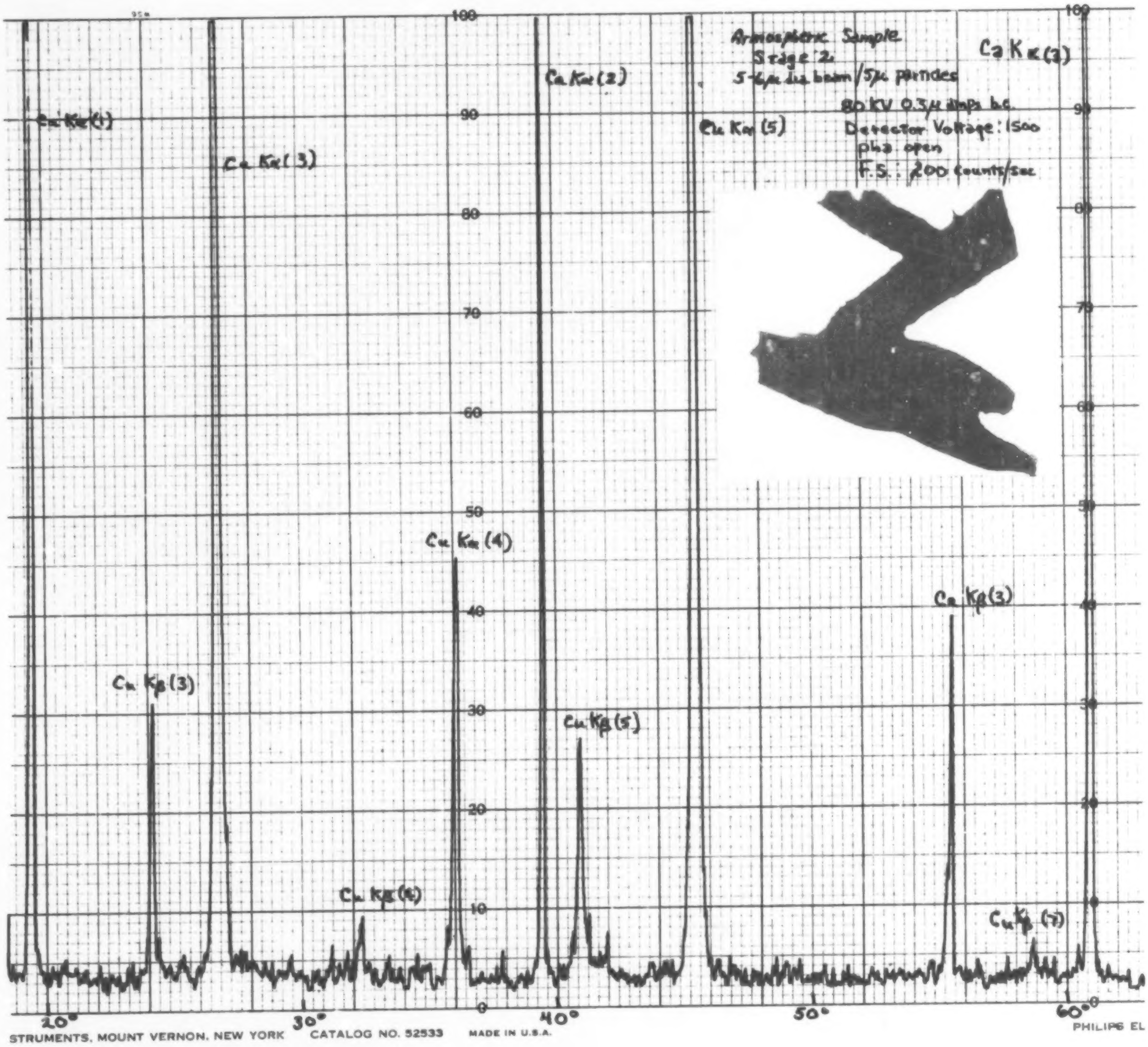

Fig. 9 Spectral Pattern from a 5μ Ca rich Particle

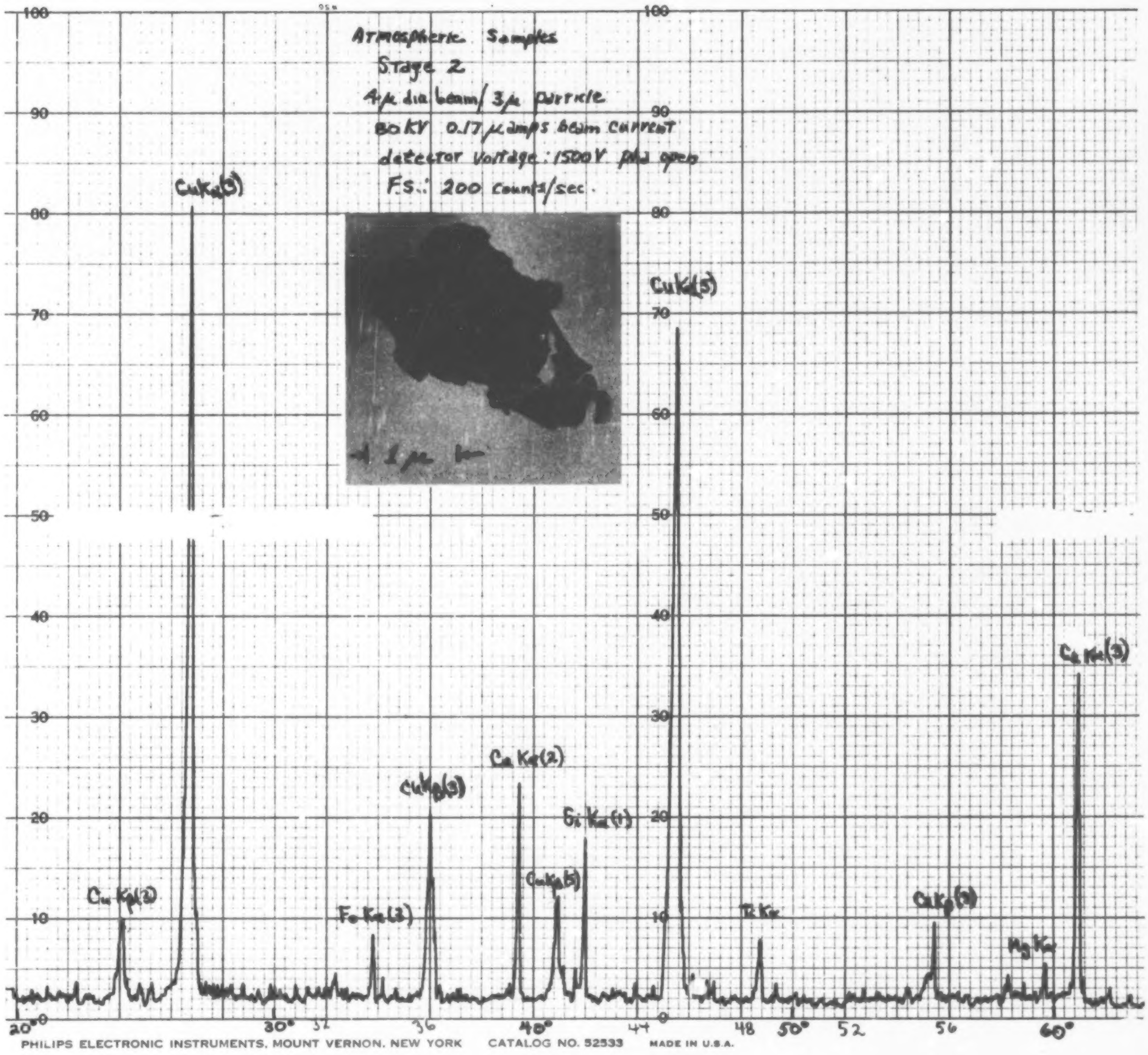

Fig. 10 Spectral Pattern from a 3μ Particle containing Fe, Mg, Ti, Ca and Si

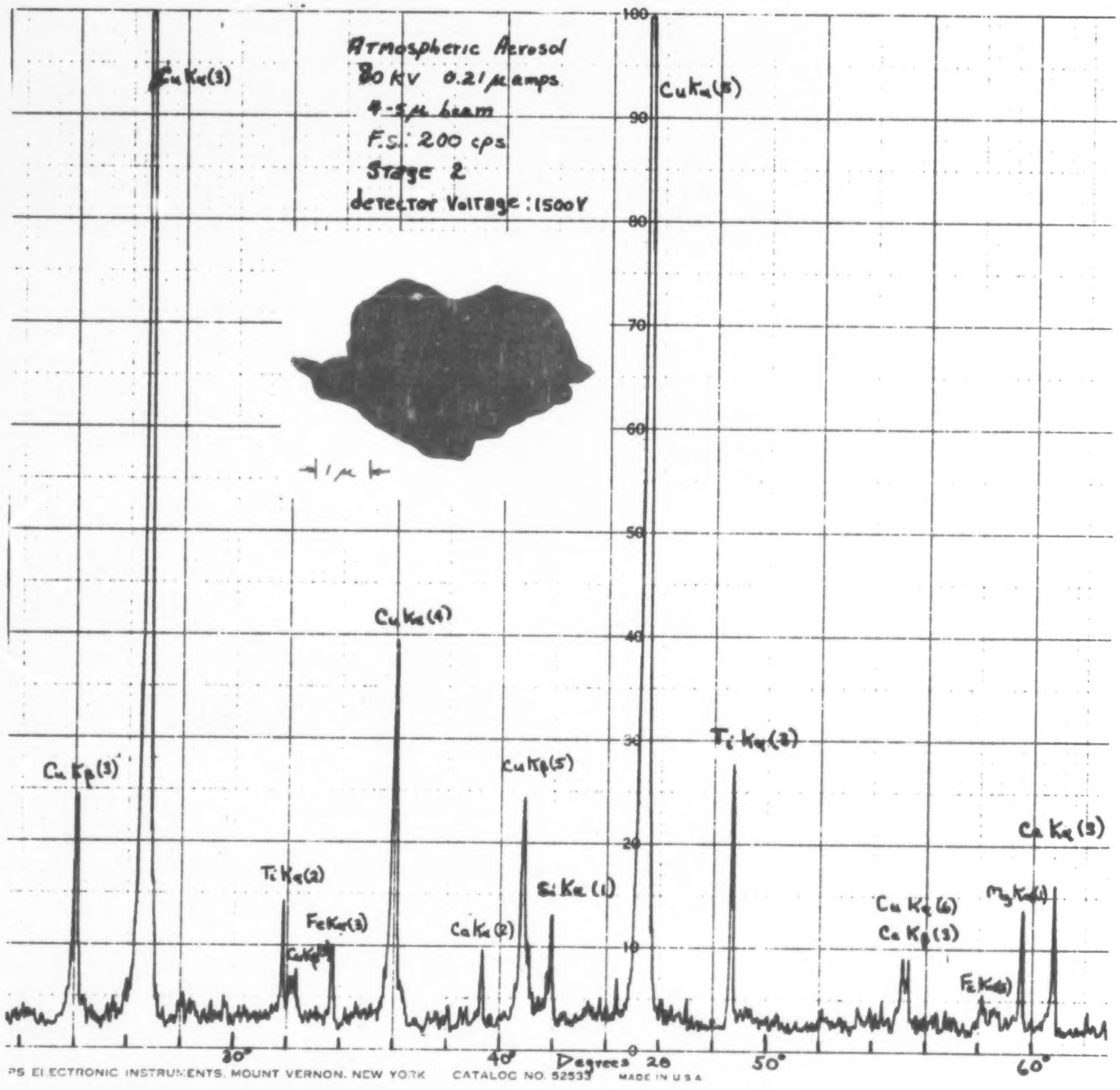

Fig. 11 Spectral Pattern from a 4μ Particle Containing Fe, Mg, Ti, Ca and Si

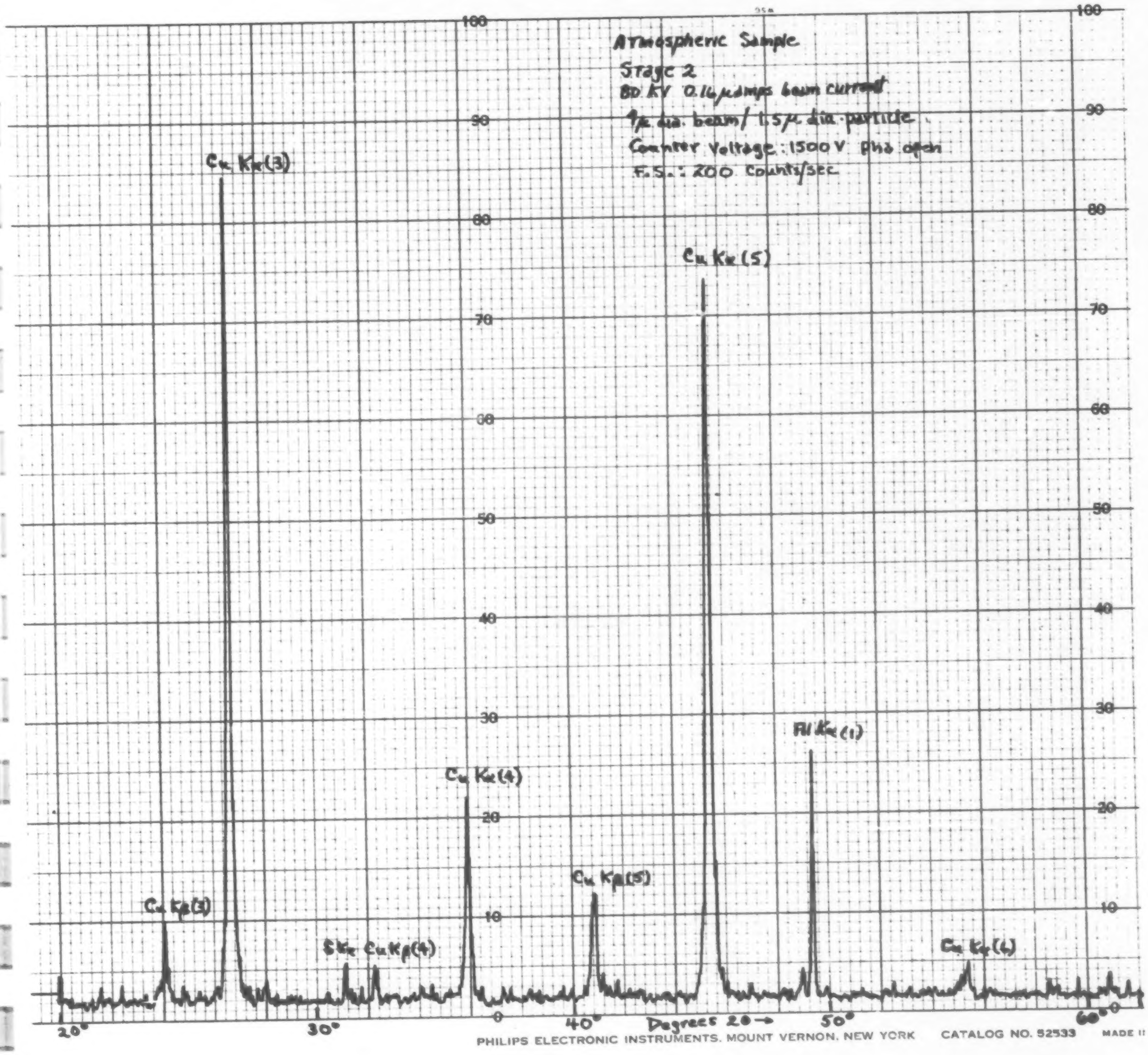

Fig. 12 Spectral Pattern from a 1.5μ Al Rich Particle

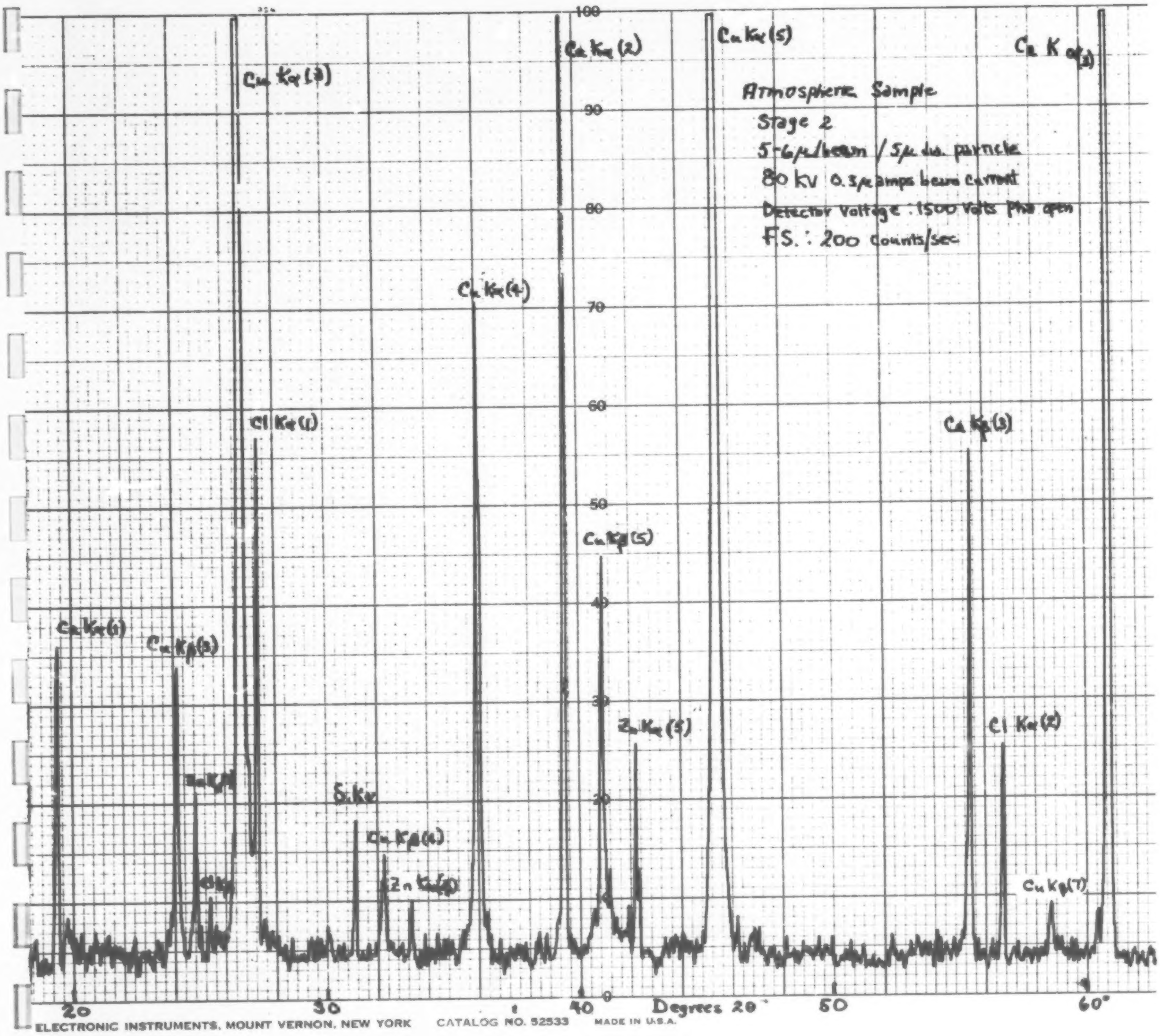

Fig. 13 Spectral Pattern from a 5μ Particle rich in Ca, Cl, Zn and S

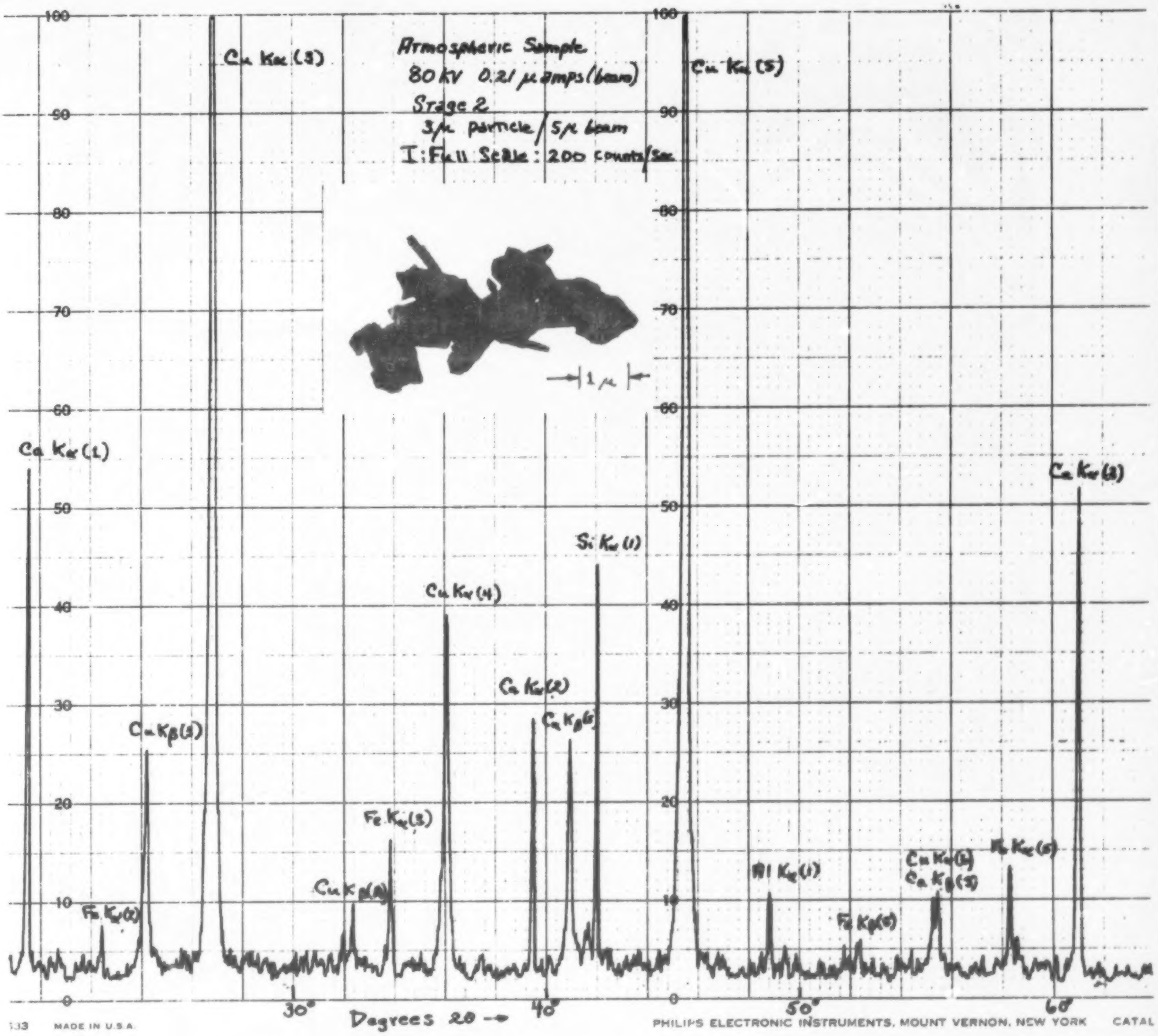

Fig. 14 Spectral Pattern from a 5μ Particle containing Fe, Ca, Al, and Si

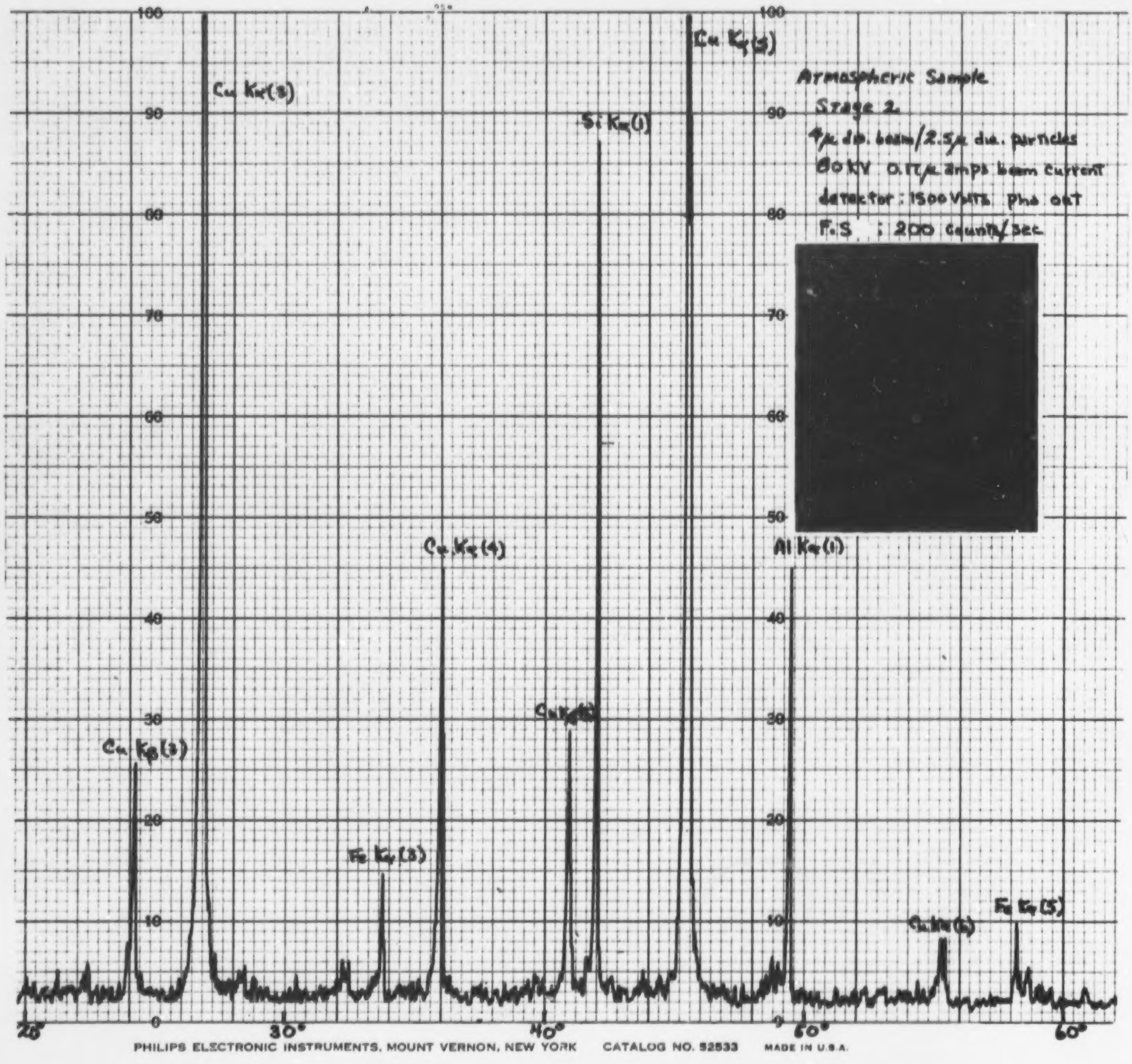

Fig. 15 Spectral Pattern from 2.5μ dia. Spherical Particles Containing Fe, Al and Si

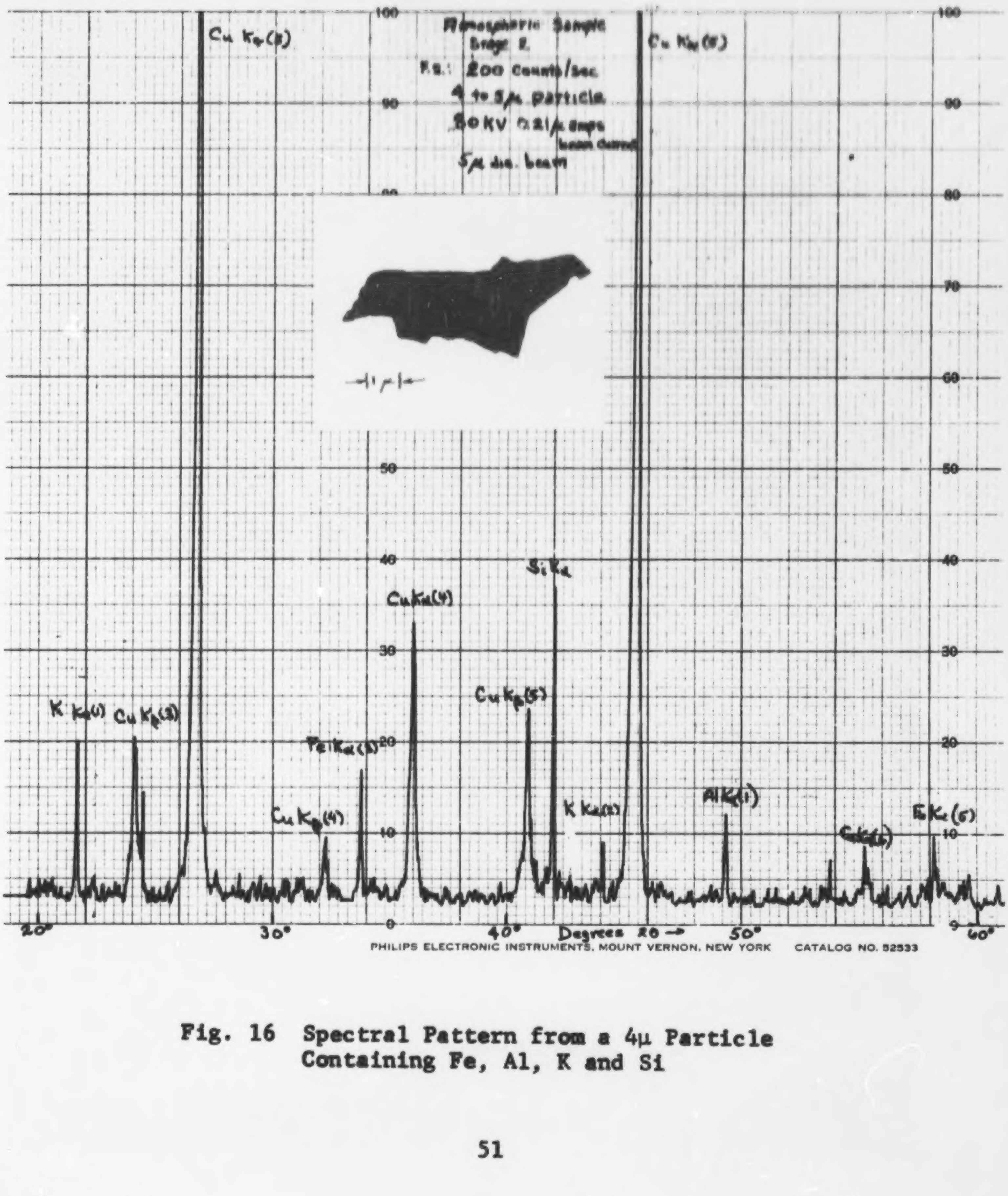

Fig. 16 Spectral Pattern from a 4μ Particle Containing Fe, Al, K and Si

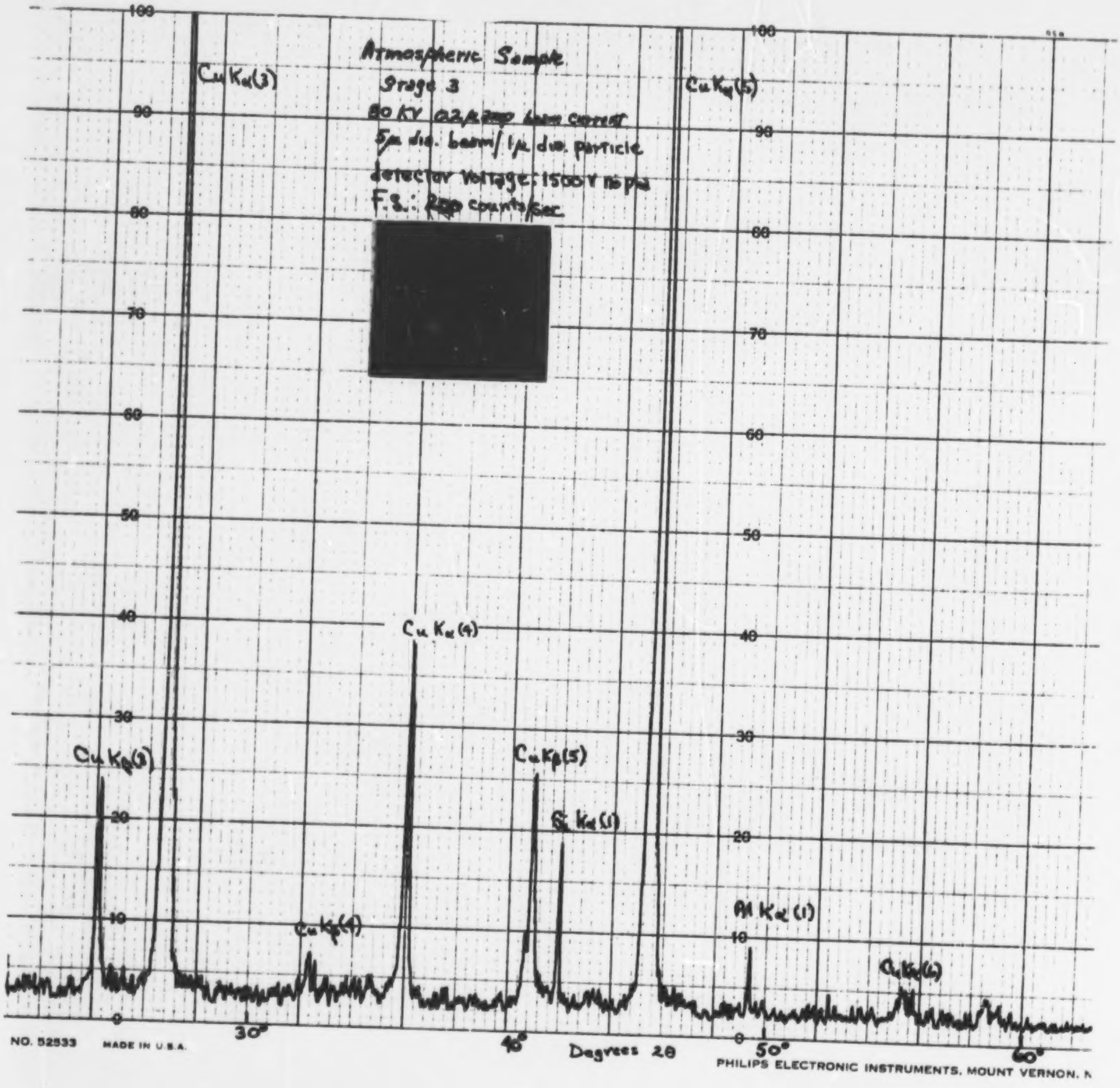

Fig. 17 Spectral Pattern from a Particle Containing Al and Si

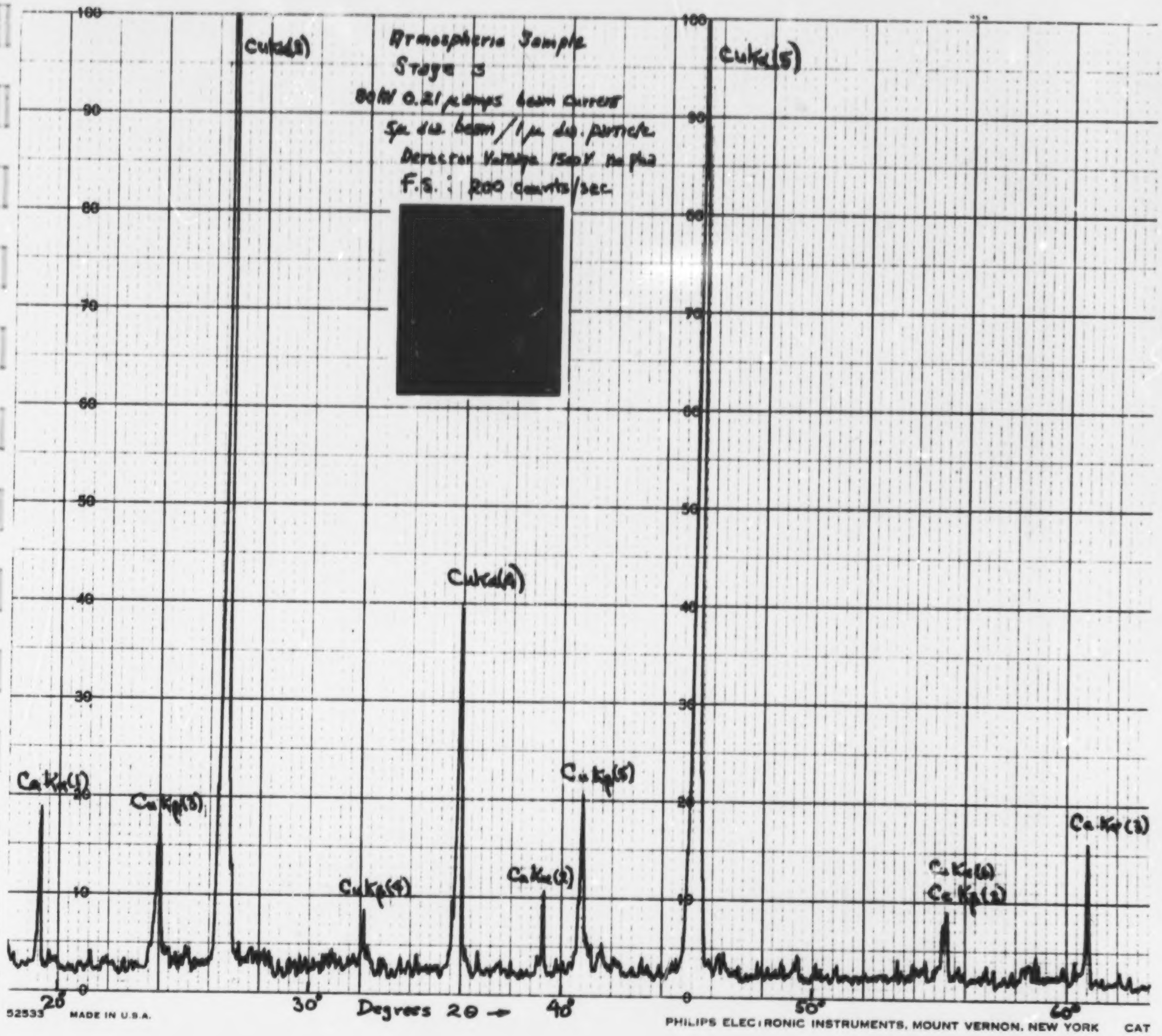

Fig. 18 Spectral Pattern from a 1μ Ca rich Particle

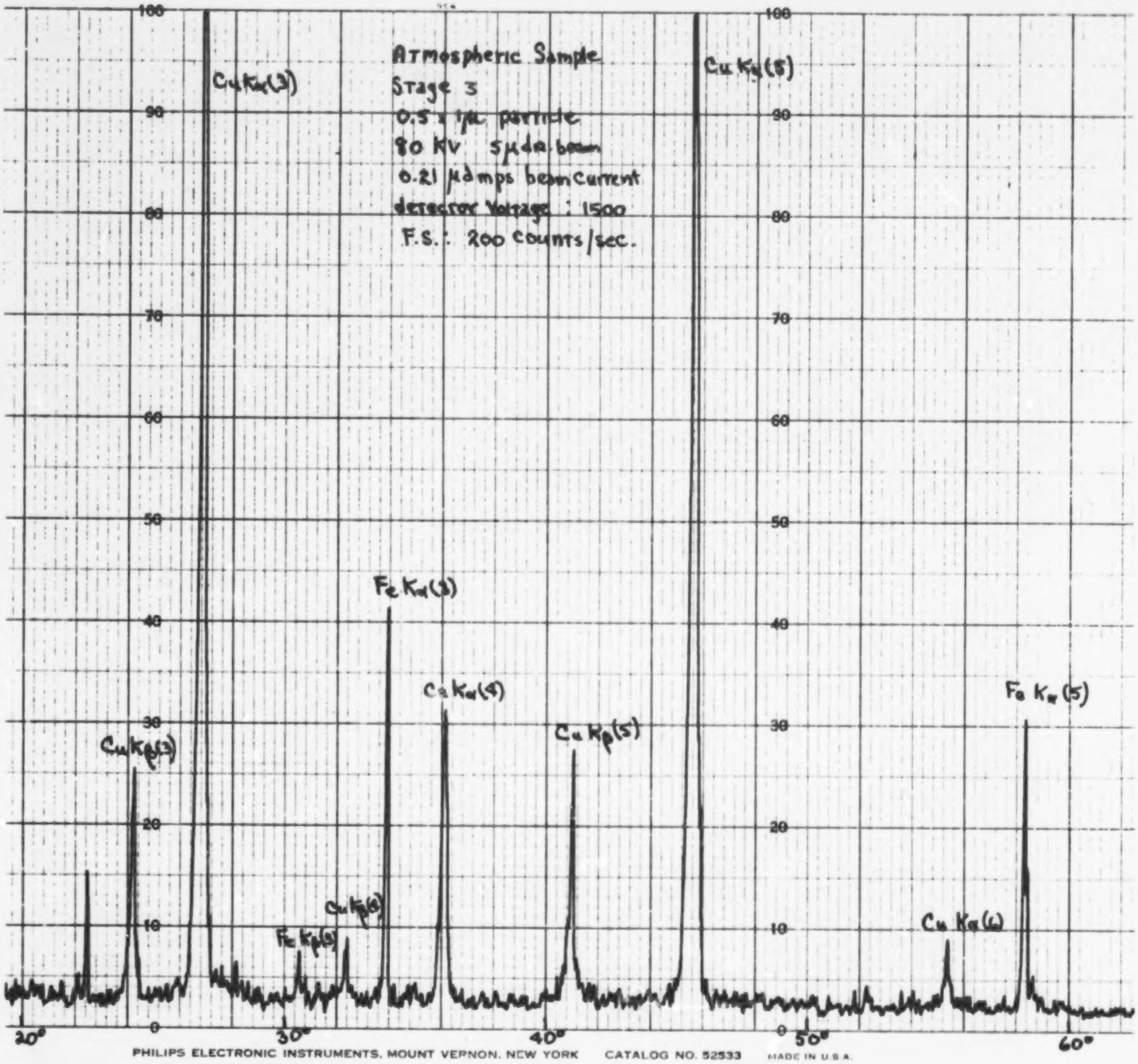

Fig. 19 Spectral Pattern from a 0.5-1μ Fe Rich Particle

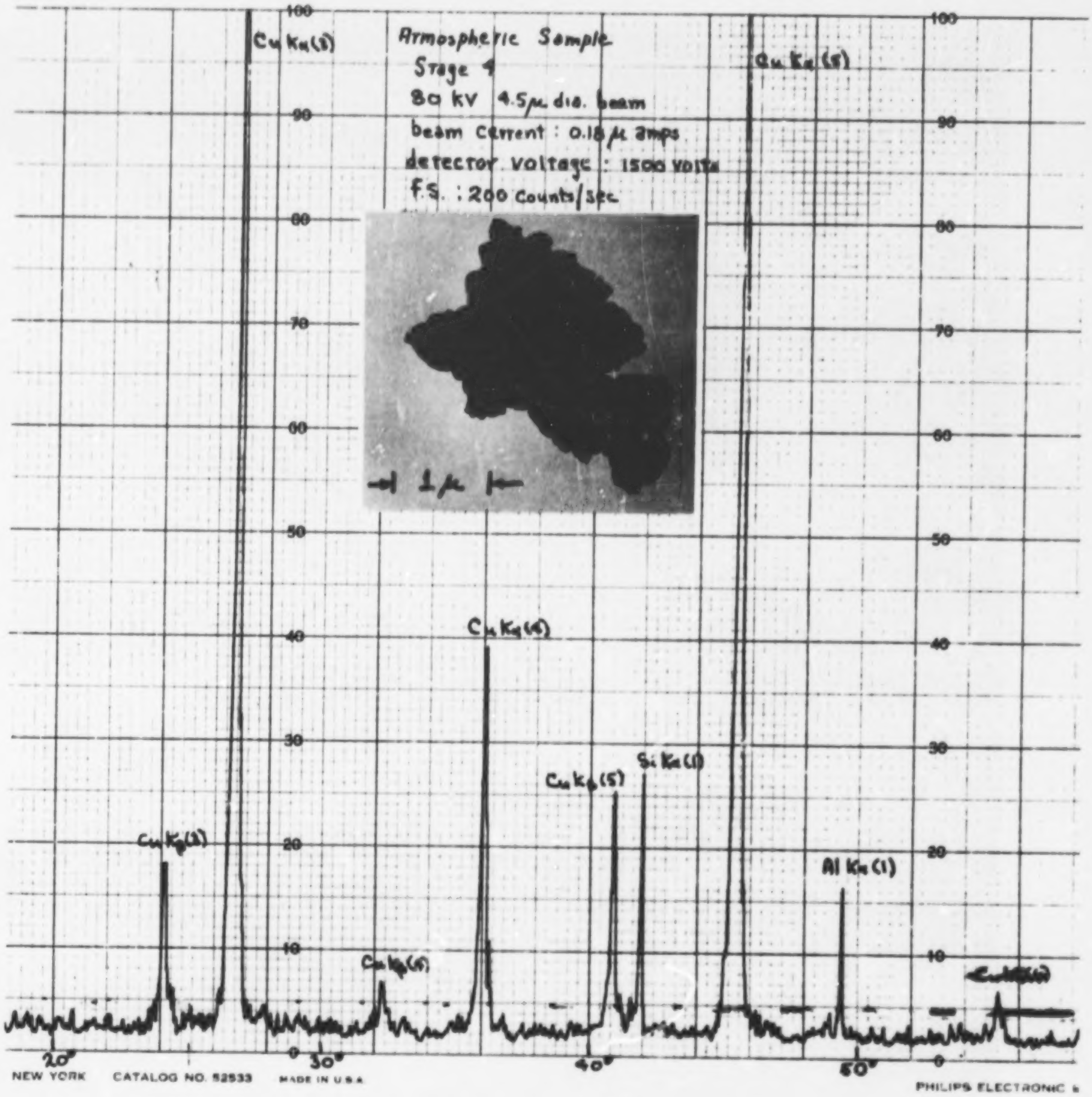

Fig. 20 Spectral Pattern from a 2μ Particle rich in Al and Si

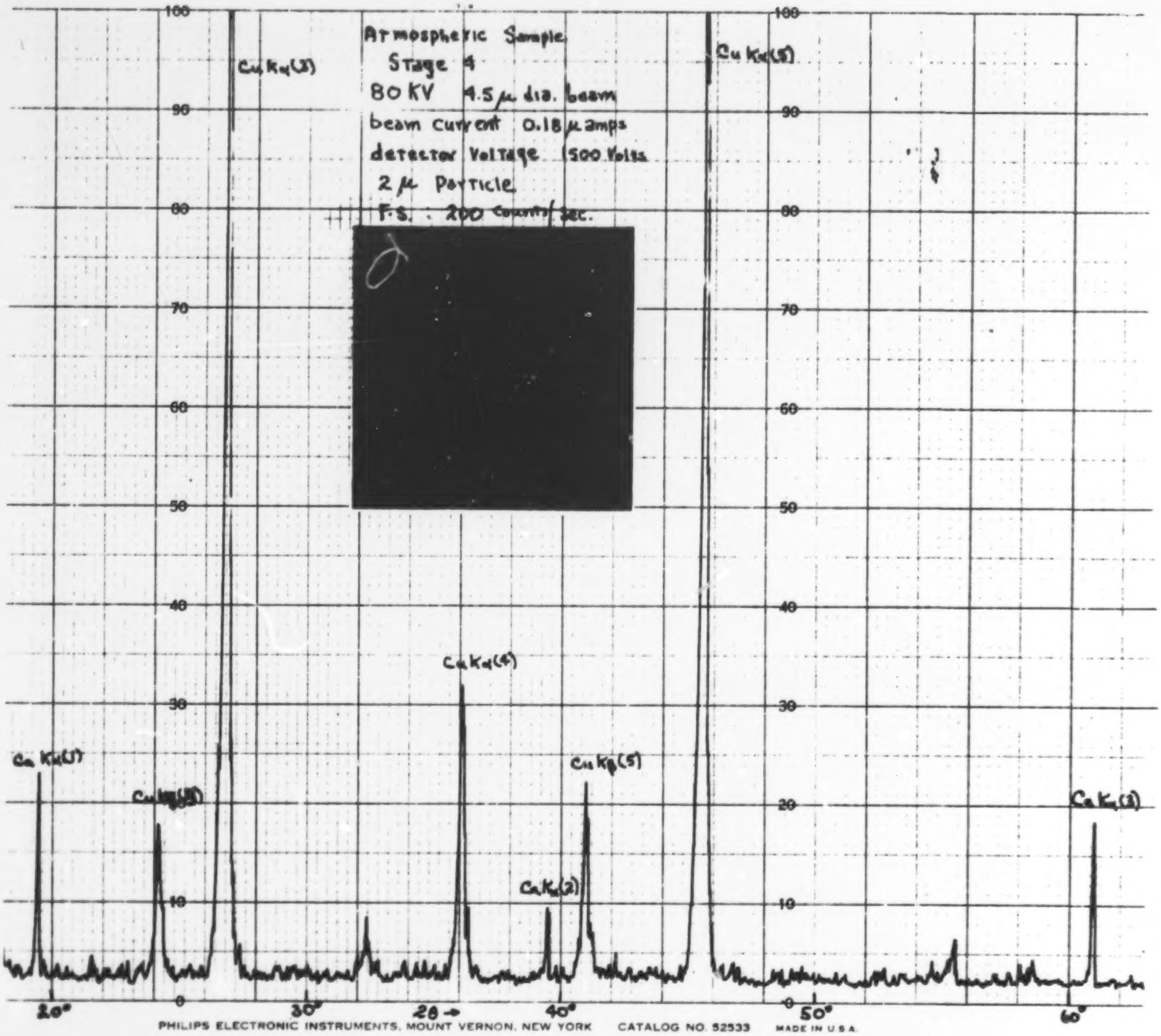

Fig. 21 Spectral Pattern from a 2μ Ca rich Particle

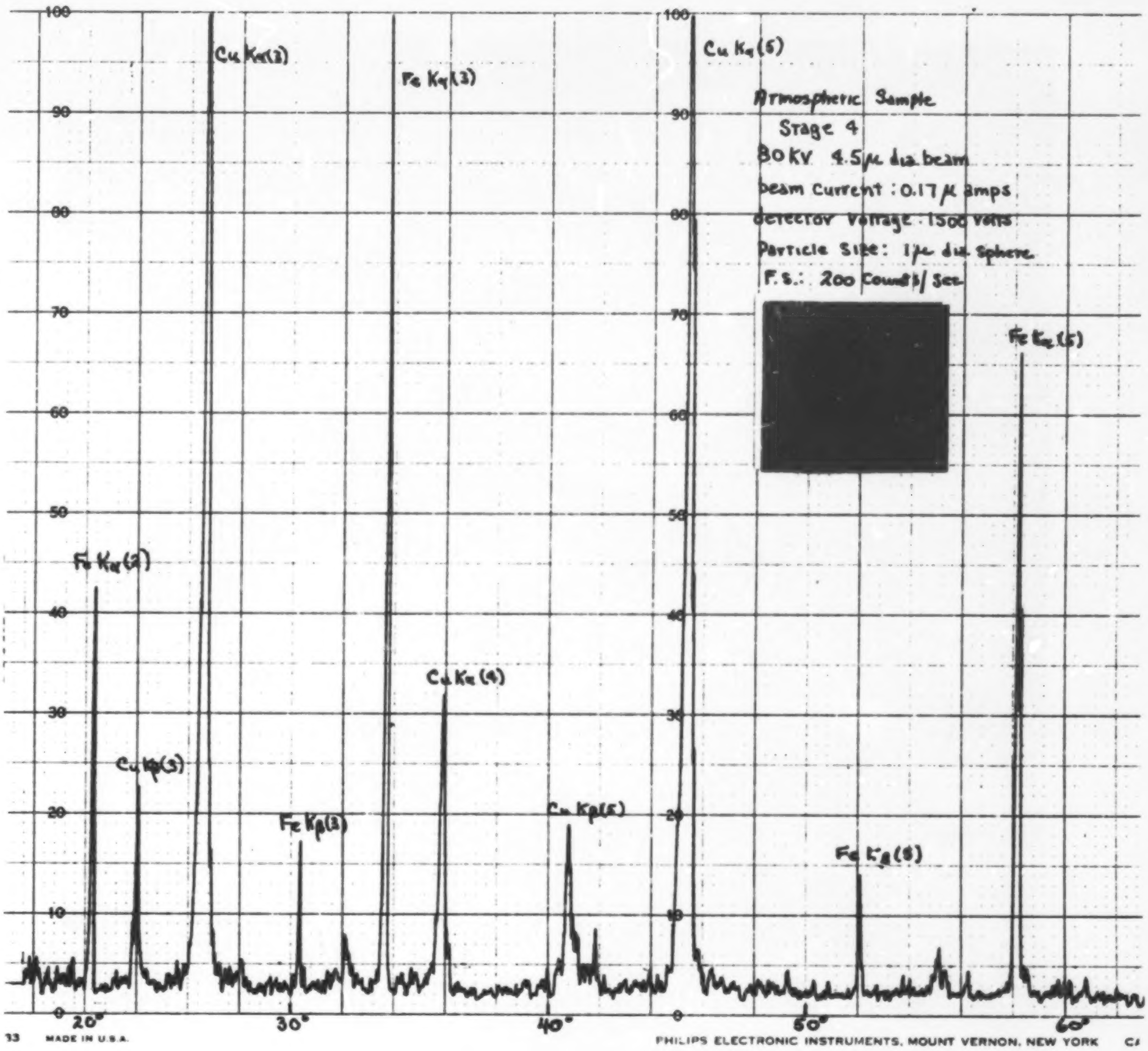

Fig. 22 Spectral Pattern from a 1μ dia. Fe rich Sphere

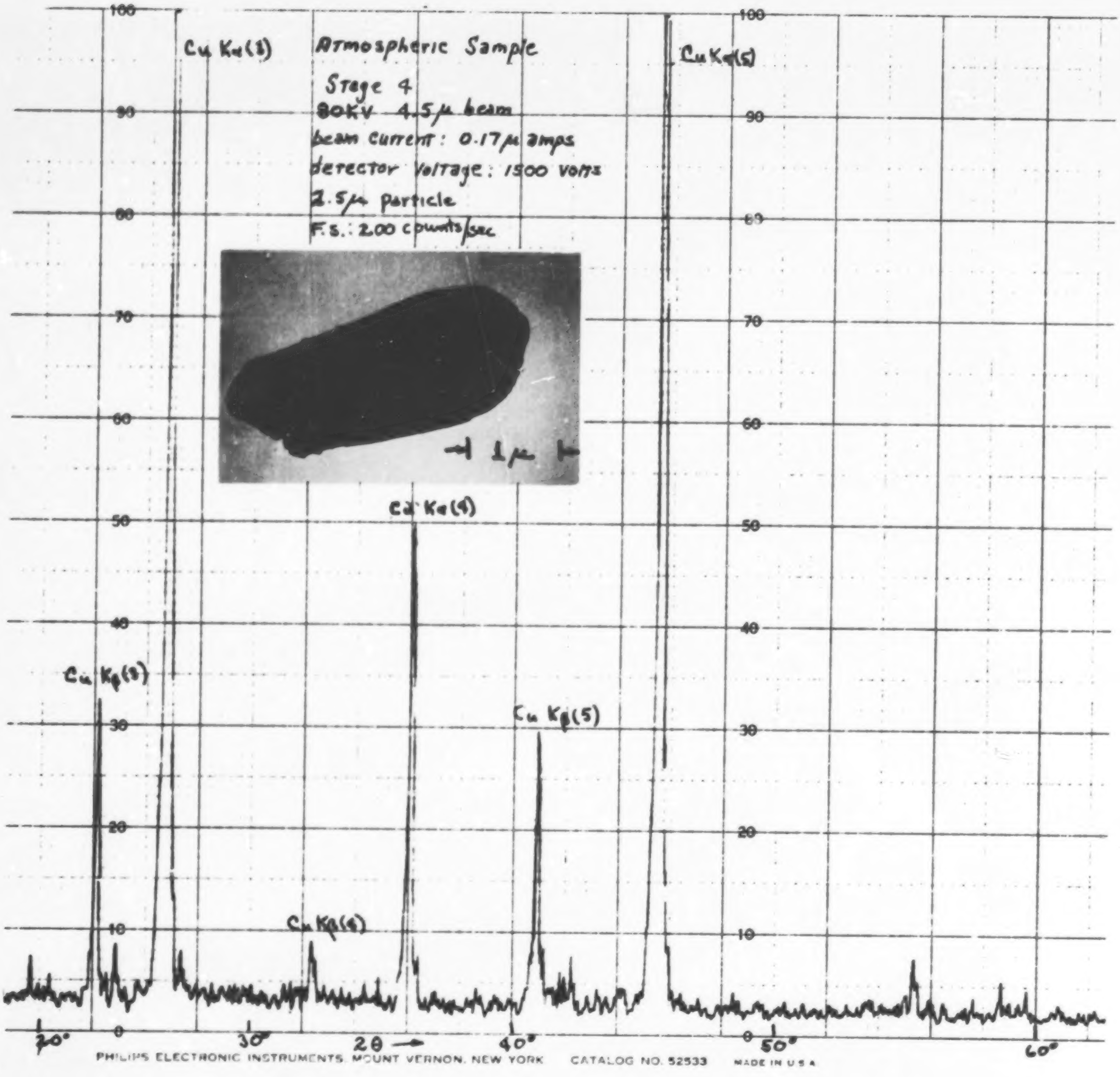

Fig. 23 Spectral Pattern from a 2.5μ Particle

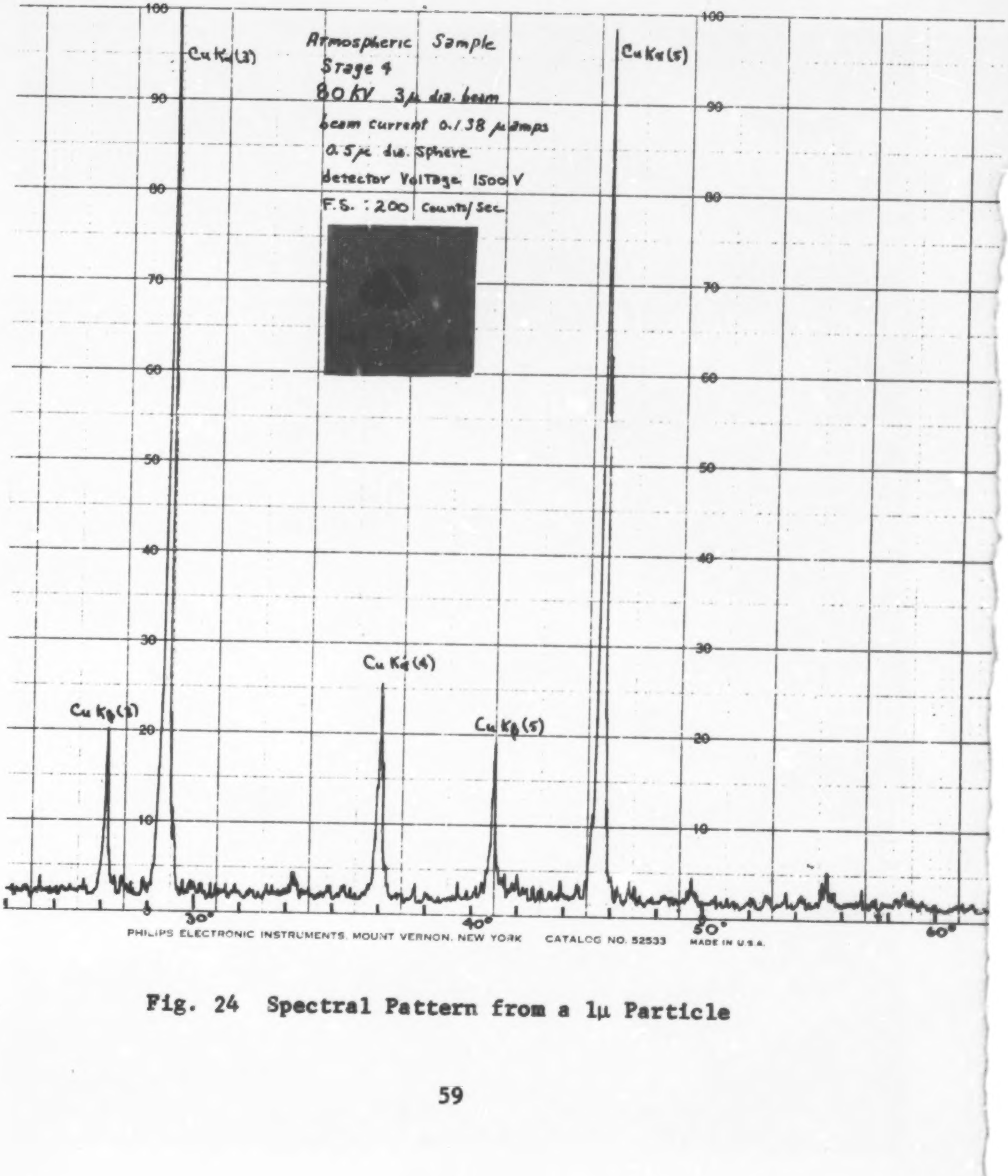

Atmospheric Sample
Stage 4
80 kV 3μ dia. beam
beam current 0.138 μ amps
0.5μ dia. Sphere
detector Voltage 1500 V
F.S. : 200 Counts/Sec

Fig. 24 Spectral Pattern from a 1μ Particle

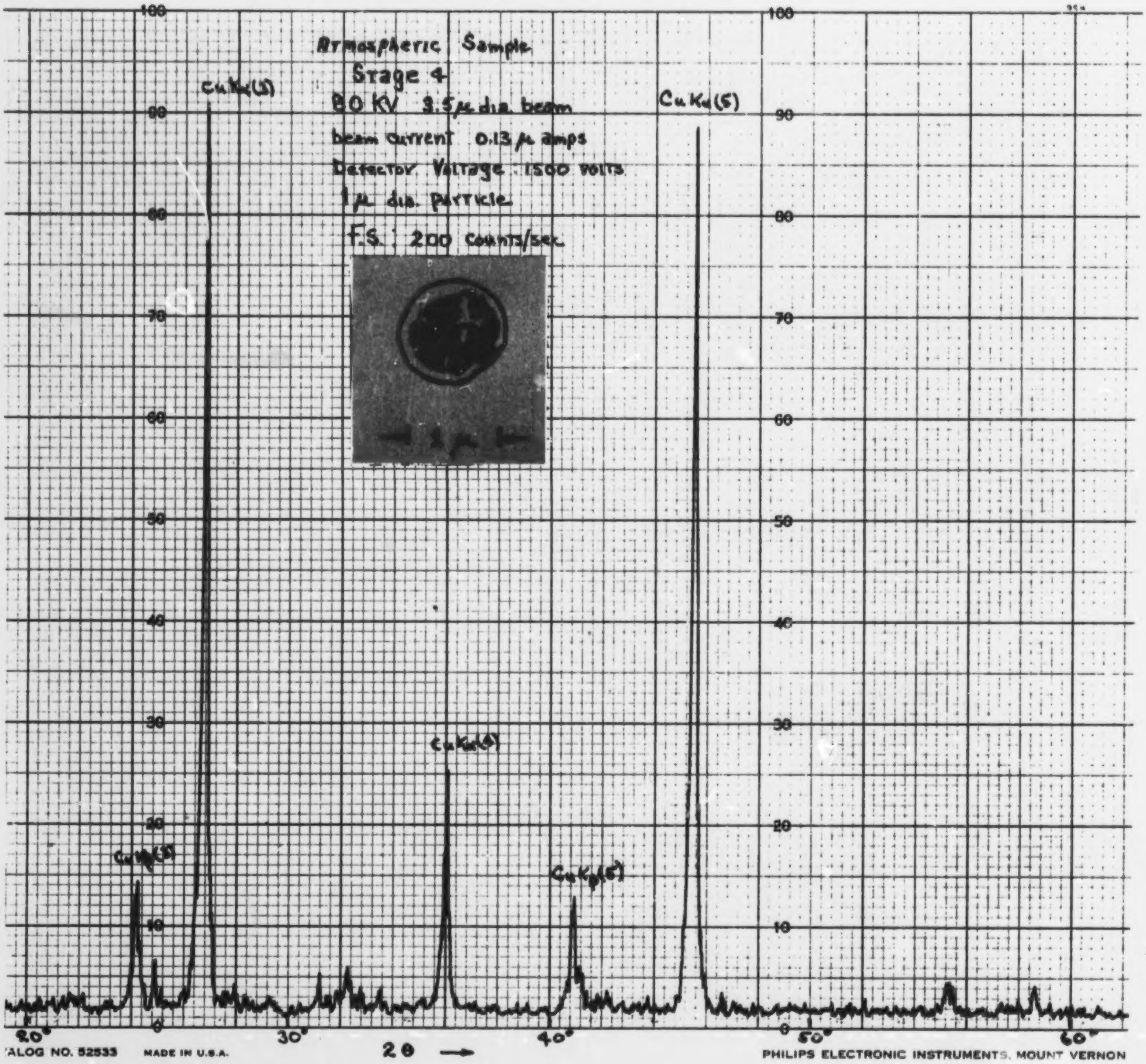

Fig. 25 Spectral Pattern from a 1μ dia. Particle

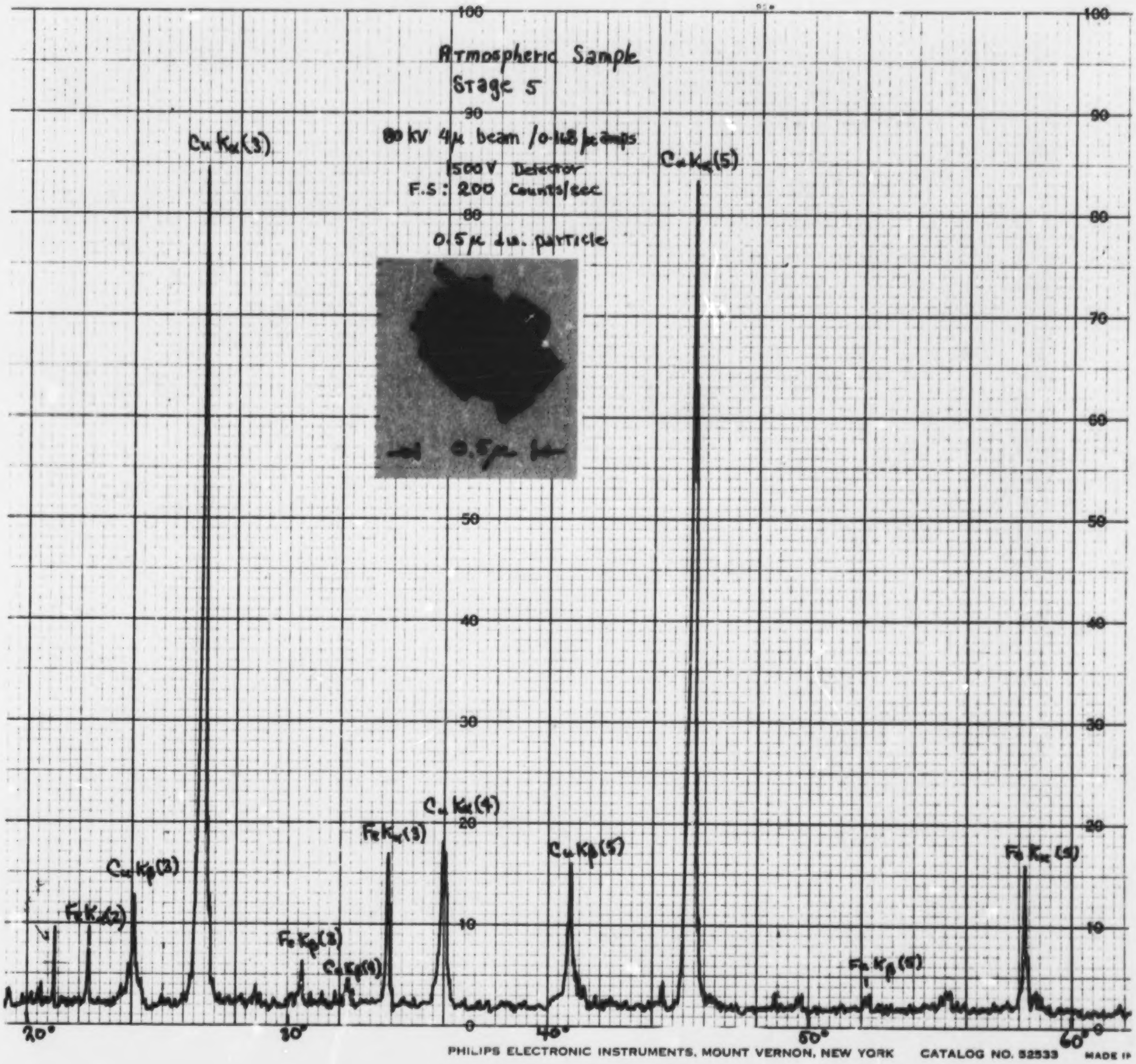

Fig. 26 Spectral Pattern from a 0.5μ Fe rich Particle

elements identified in the particulates were Al, K, Zn, S, Ti and Cl. Table 14 summarizes the results of the spectral patterns, with the major elements designated. Based on the intensity obtained from semi-infinite pure samples at 30 KV, the relative proportion of each element in the particles is estimated. It should be noted that these values are at best an estimate, since the spectral patterns were obtained at 80 KV, the particles are not semi-infinite in extent, and no attempt has been made to correct for absorption effects. Nevertheless, this approach does serve to weight the intensities available from the characteristic lines of different elements to establish a more reasonable basis for estimating the amount of each element present. Since light elements cannot be detected, the results have been normalized to 100% of the elements detected. The results obtained from Electron Beam Microanalysis are included in this table as well as the results obtained from the spectral patterns of particles from stages 3, 4, and 5, respectively. The latter are shown in Figs. 17 through 26. Particulate matter on these stages was found to be similar to that observed on stage 2 with the exception that the spectral patterns from many particles exhibited no characteristic lines (See Figs. 23, 24 and 25). In general, the fairly large particles (greater than 1 micron) which were found on collections from the higher stages (Stage 4 and 5) of the impactor contained no heavy elements, indicating that these particles are light element compounds (C, O, N, etc.). Very few particles were observed on stage 5 of the collection. In addition, most of those observed yielded no spectral lines. A spectral pattern was obtained from one particle 0.5 microns in size (See Fig. 26), indicating sufficient detectability was available to establish the presence of many of the elements observed in the lower stages. As a result, it is believed that many of the particles on this stage ($\geqq$0.5 microns) are light element compounds. These results are in keeping with those obtained from the Electron Beam Microanalyzer, where the average analysis of Stage 4 particulates revealed the presence of C, O and S, with traces of Fe and Si.

The results presented in Table 14 show that the same elements were observed employing either the Electron Beam Microanalyzer or the Electron Microscope. Because optical magnifications in the microprobe are limited to 300 to 400X, particles could only be distinguished as motes on the Be substrate. Nevertheless, microprobe analysis of these particles revealed that they consisted predominately of Ca, Si and Fe. Some particles strongly indicated the presence of Ti and Mg. Since

Table 14

Major Element Present in Atmospheric Aerosol Collection

Electron Beam Microanalyzer (Stage 3)

Ref.	Major Elements
Particle 1	20% Si, 80% Fe
Particle 2	60% Ca, 35% Si, 5% Al
Particle 3	21% Ca, 50% Fe, 29% Si
Particle 4	25% Ca, 75% Fe
Particle 5	49% Ti, 32% Fe, 19% Ca
Particle 6	34% Ca, 27% Fe, 28% Si, 11% Al
Particle 7	19% Ca, 36% Fe, 44% Si
Particle 8	6% Ca, 75% Fe, 20% Si

EM 200 Electron Microscope/Spectrometer Attachment

Ref.	Particle Size	Stage	Major Elements
Fig. 3-6	2μ sphere	2	Fe (17%), Si (60%), Al (22%)
Fig. 7	4μ	2	Ca
Fig. 8	1μ	2	Ca
Fig. 9	5μ	2	Ca
Fig. 10	3μ	2	Ca (52%), Si (28%), Fe (9%) Ti (6%), Mg (5%)
Fig. 11	4μ	2	Ca (23%), Si (16%), Fe (13%) Ti (27%), Mg (20%)
Fig. 12	1.5μ	2	Al (86%), S (14%)
Fig. 13	5μ	2	Ca (25%), Cl (41%), Zn (25%), S (10%)
Fig. 14	5μ	2	Ca (45%), Fe (12%), Al (7%), Si (37%)
Fig. 15	2.5μ	2	Fe (9%), Al (32%), Si (59%)

Table 14 (Cont'd.)

Ref.	Particle Size	Stage	Major Elements
Fig. 16	4μ	2	K (20%), Fe (20%), Al (13%) Si (48%)
Fig. 17	1μ	3	Al (30%), Si (70%)
Fig. 18	1μ	3	Ca
Fig. 19	0.5 x 1μ	3	Fe
Fig. 20	2μ	4	Al (38%), Si (62%)
Fig. 21	2μ	4	Ca
Fig. 22	1μ	4	Fe
Fig. 26	0.5μ	5	Fe

in the electron microscope, particles can be viewed at magnifications up to 200 times that which is available in the Microanalyzer, it is possible to determine the elements comprising individual particles with a far greater degree of confidence. As a result, the presence of Fe and Si was completely confirmed in the Electron Microscope and there is no question that these elements comprise an important part of many of the particles examined.

To summarize, the atmospheric samples could be characterized by the fact that a large number of different compounds are present, e.g. there is evidence for the possible presence of: CaO or $CaCO_3$ (Ca-rich particles); Ca(Fe, Mg, Ti) silicates; Fe or Fe oxide; Ca (Fe, Al) silicates; Al (Fe) silicates; Al oxide; Al (Fe,K) silicates; $CaCl_2$; and ZnS, or other zinc sulfur compounds. In addition to these compounds which were found to populate the lower stages of the impactor, light element compounds (C, O, S, etc.) were found to predominate the higher stages of the impactor (Stage 4 and 5).

Previous experience in this laboratory involving the microanalysis of the combustion products of coal has revealed that these products also contained a variety of different compounds which were commonly comprised of Ca, Si, Al, Fe, Ti, K, Na, and S. It is interesting to note that the results obtained from the atmospheric aerosols strongly parallel those obtained from the coal combustion products, indicating the latter as a possible source of the atmospheric aerosol contaminants.

3. Scanning Electron Microscopy

Although the electron photomicrographs were adequate for the observation of particle shape, they are essentially shadowgraphs and furnish very little topographical information. The results obtained from the Scanning Electron Microscope are far superior for this purpose. Figs. 27 and 28 are Scanning Electron photomicrographs obtained from Stages 3 and 5 of the collection.

In addition to topographical information, the different particle types from Stage 3 can be readily recognized, e.g. spherical particles can be seen adhering to more flocculent matter (See Figs. 27e and 27g). The presence of organic matter is also easily distinguished as evidenced by the perfect hexagonal array or "honeycomb" shown in Fig. 27f. In addition to particulate matter, Scanning Electron Microscopy revealed the presence of stained areas on the Be substrate (See Fig. 28a and b). Higher magnification of these areas had a peculiar cratered appearance (Fig. 28g and 28h) which could have been caused by chemical action of droplets of a corrosive liquid. Since sulfuric acid is believed to be a component of atmospheric contamination and since sulfur was detected in the Electron Beam Microanalyzer, there is evidence to substantiate this interpretation.

D. Auto Exhaust Samples

Specimens from the auto exhaust collections were examined in the Electron Beam Microanalyzer and in the Electron Microscope. As in the case of the atmospheric aerosol, the particles to be analyzed in the microprobe were mounted on polished Be discs, while those scheduled for analysis in the Electron Microscope were mounted on standard Cu grids.

These samples differed greatly from the atmospheric collections in that the density of particulate matter was extremely low. No particles could be discerned on the Be discs in the optical microscope at 1000X. Stained areas could be seen, which may have been caused by condensation from the exhaust stream. The inability to see particles optically, coupled with the sparsity of particulate matter made analysis in the Microanalyzer extremely difficult. The spectrometers were aligned to detect Pb and Cl and a search was made on the surface of the Be discs. Stages 4, 5 and the back-up electrostatic precipitor were examined. No evidence of these elements could be detected.

Examination in the electron microscope confirmed that very few particles were present and that the average particle size on stage 4 was of the order of 0.1 microns. Particles on the back-up electrostatic precipitator were found to be less than or equal 0.1 microns in size. Attempts to analyze these particles for Pb in the electron microscope proved to be fruitless, both by employing the spectrometer attachment or by non-dispersive analysis. As a result, one must conclude that if Pb is present in these particles, the detection of x-rays from particles of this size lies beyond the present analytical capability of the technique. Based on the results obtained from the electron microanalysis of semi-infinite samples, this conclusion is not unreasonable. Since the mass of a particle 0.1 micron in size is approximately 1×10^{-4} of the excitation mass (at 30 KV) available from a semi-infinite sample, the x-ray intensity available from the particle would be reduced in the same proportion. From microprobe experience,

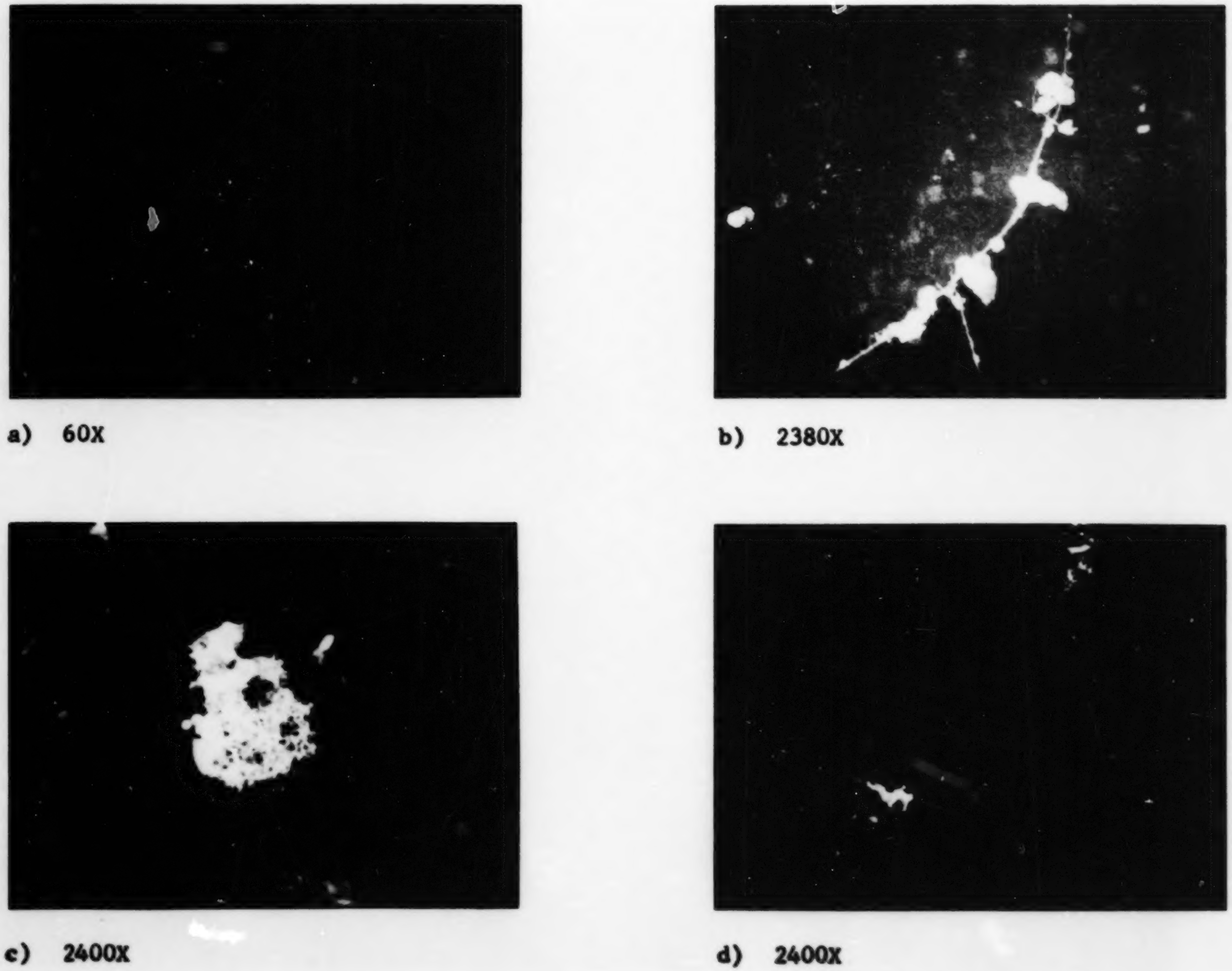

a) 60X

b) 2380X

c) 2400X

d) 2400X

Fig. 27 Scanning Electron Microscopy of Air Pollution Sample

Stage 3

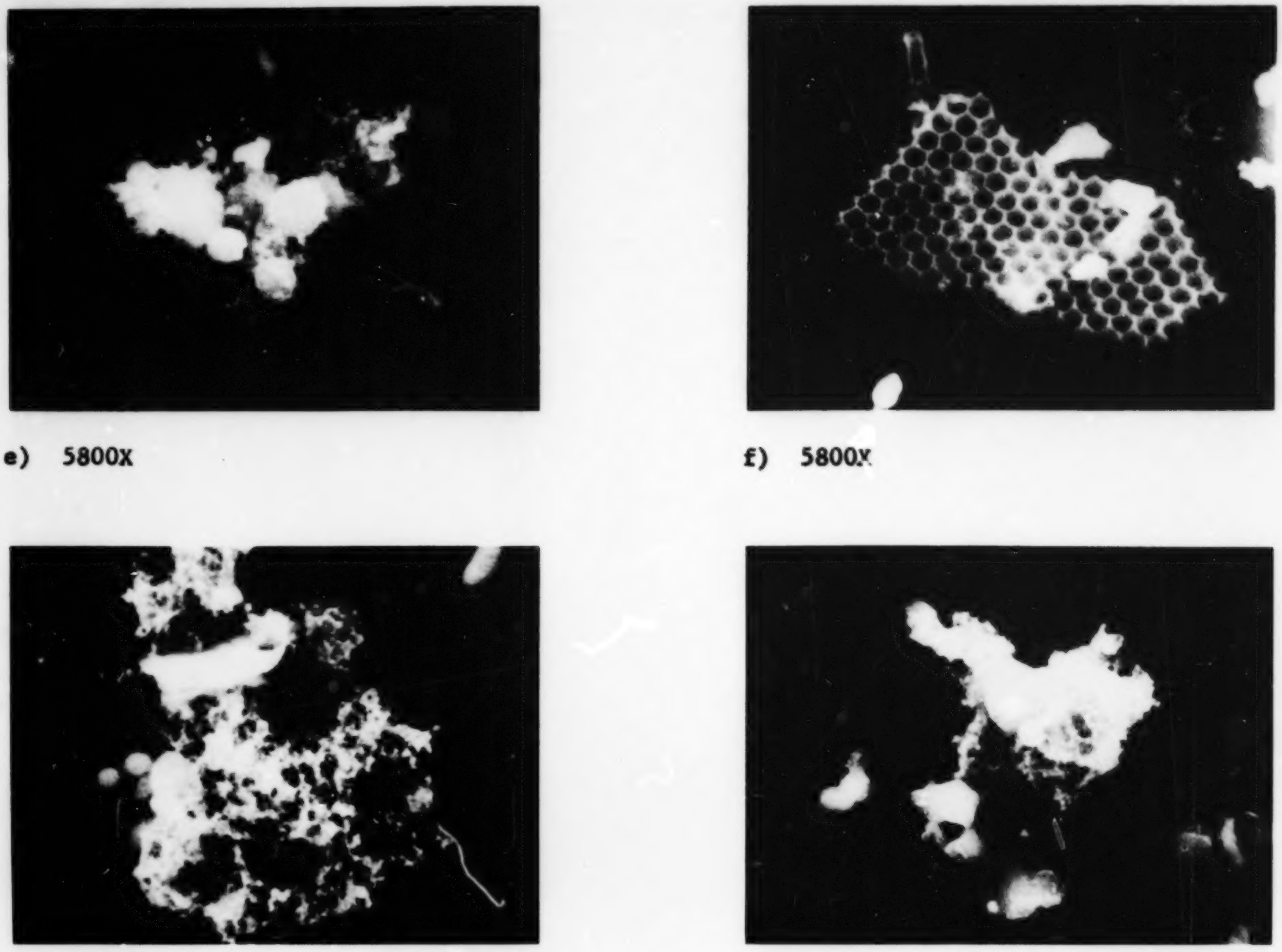

e) 5800X

f) 5800X

g) 5800X

h) 5800X

Fig. 27 cont. Scanning Electron Microscopy of Air Pollution Sample
Stage 3

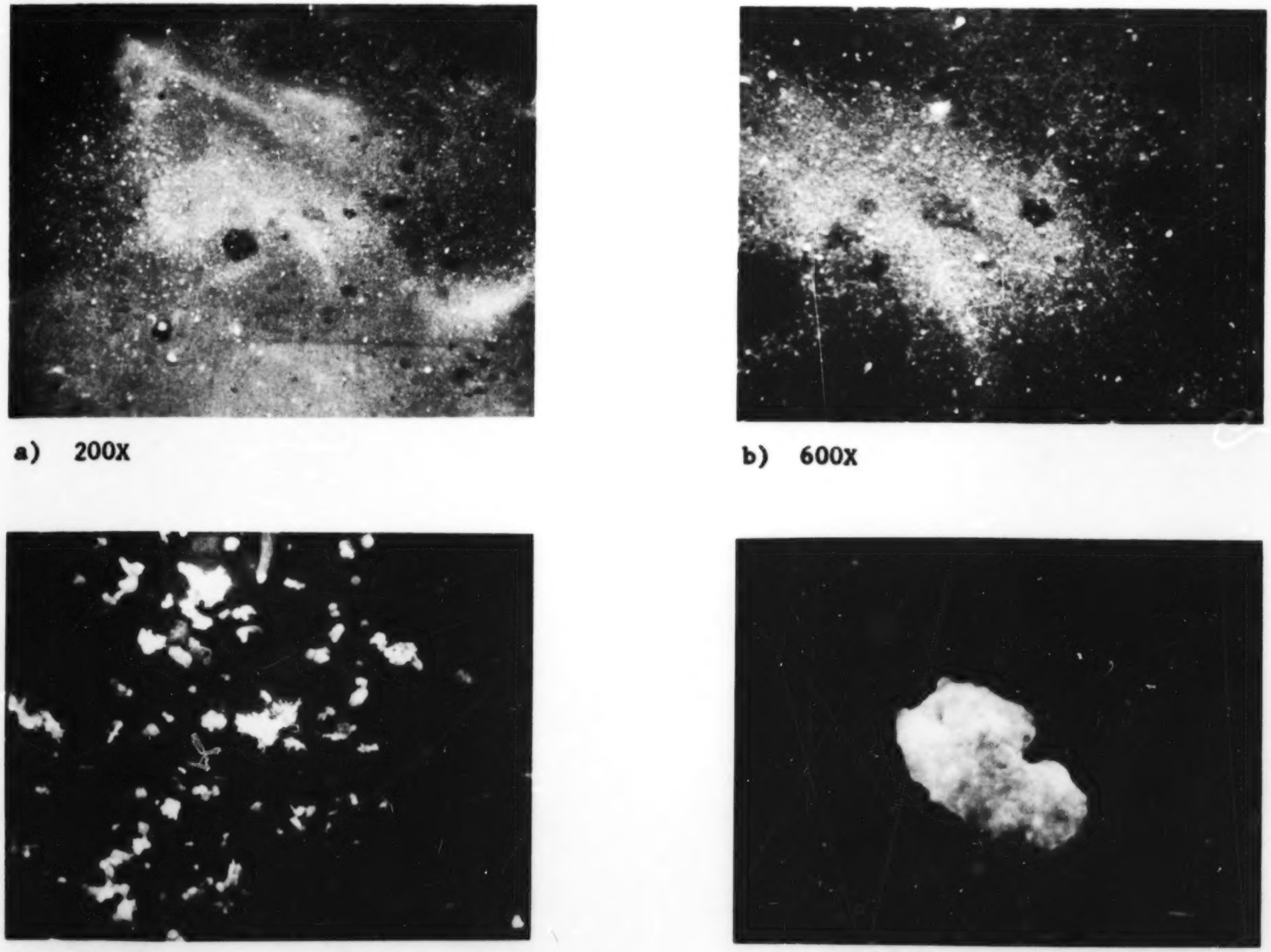

a) 200X

b) 600X

c) 1180X

d) 5800X

Fig. 28 Scanning Electron Microscopy of Air Pollution Sample
Stage 5

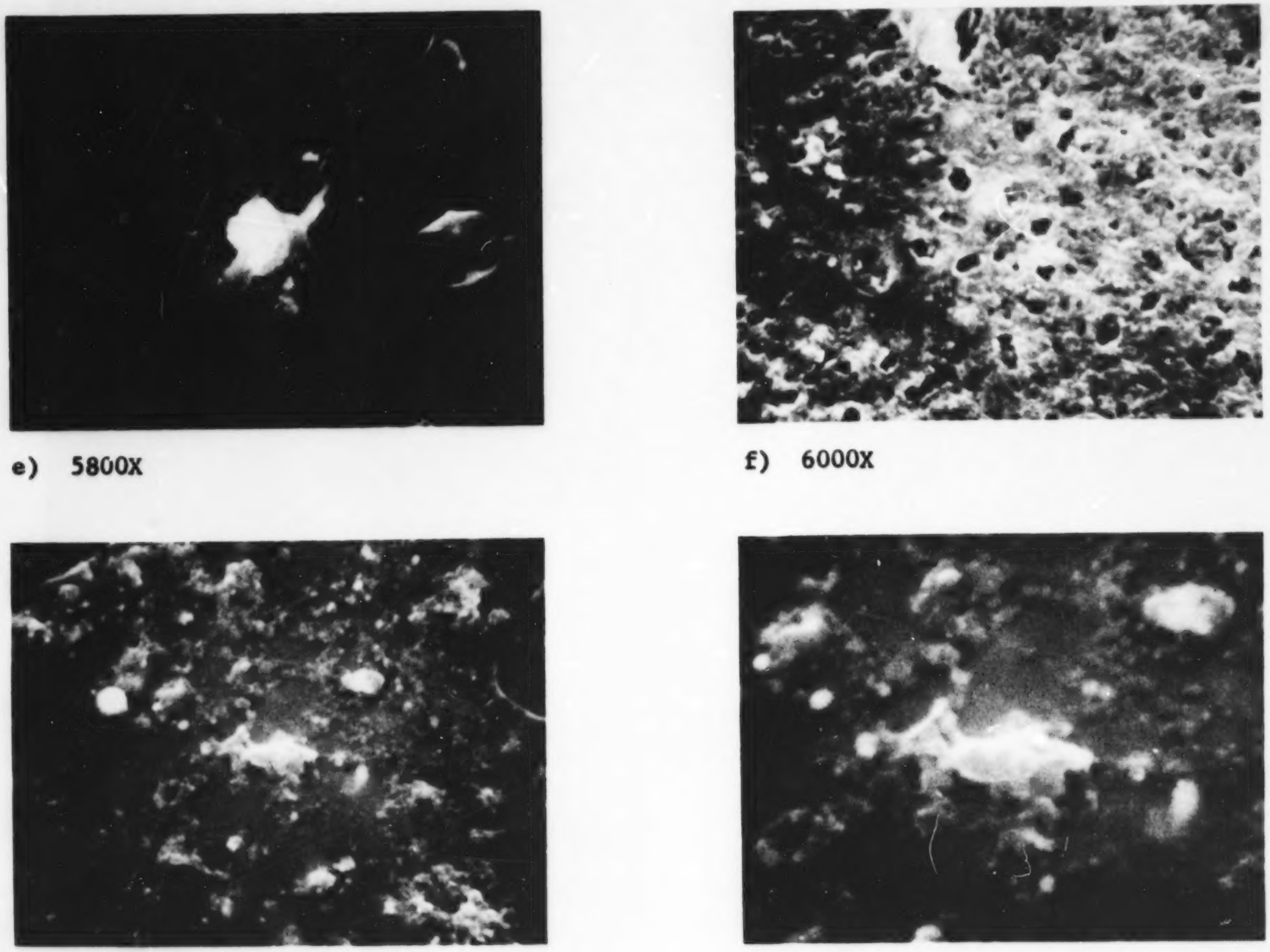

e) 5800X

f) 6000X

g) 6000X

h) 12000X

Fig. 28 cont. Scanning Electron Microscopy of Air Pollution Sample
Stage 5

the PbLα x-ray intensity available from a semi-infinite sample at 30 KV electron acceleration potential is in the vicinity of 1500 counts per second with a signal to noise ratio of 1000/1. Assuming a detectability limit equivalent to twice the signal to noise ratio, the minimum signal detectable would be the order of 3 counts per second. Since the signal available from the 0.1 micron particle would only be 0.15 counts per second, particles of this size cannot be detected. Assuming the particle is 100% Pb, the minimum measurable particle diameter corresponding to a detectability limit of 3 counts per second is approximately 0.25 microns. Non-dispersive analysis lowers the detectability limit such that particles of one-tenth the volume (for our system) which can be analyzed dispersively (with a spectrometer) are capable of being studied. Even employing this criterion, the minimum measurable diameter of a particle of pure Pb would be of the order of 0.12 microns, which is right on the borderline of detectability for these observed particle sizes ($\sim 0.1\mu$).

This detectability limit could be lowered in future systems by employing dispersive and/or non-dispersive x-ray detection systems which are capable of collecting a larger solid angle of x-rays from the specimen, which, in effect, can result in an increase in the x-ray available intensity.

E. Ni film specimens

Thin Ni films, approximately 1000A° thick, which had been prepared by vacuum evaporation on nitrocellulose substrates supported on standard Cu grids were examined in the EM 200 Electron Microscope and in the Scanning Electron Microscope. These films had been subjected to contact with aerosol mists of H_2SO_4, the droplets of which had been sized by the Batelle Impactor. It was hoped that holes or reaction pits would develop in the Ni film and that these could be analyzed in the electron microscope. Scanning Electron photomicrographs of these samples are shown in Figs. 29 through 32.

No evidence of reaction of the Ni with the acid was observed by either conventional or scanning electron microscopy. Surface features were observed, but these appear to be defects or structure in the Ni or the nitrocellulose film. Since the scanning electron microscope is quite sensitive to topographical features, one can only conclude that little or no reaction had occurred between the Ni and the droplets of acid.

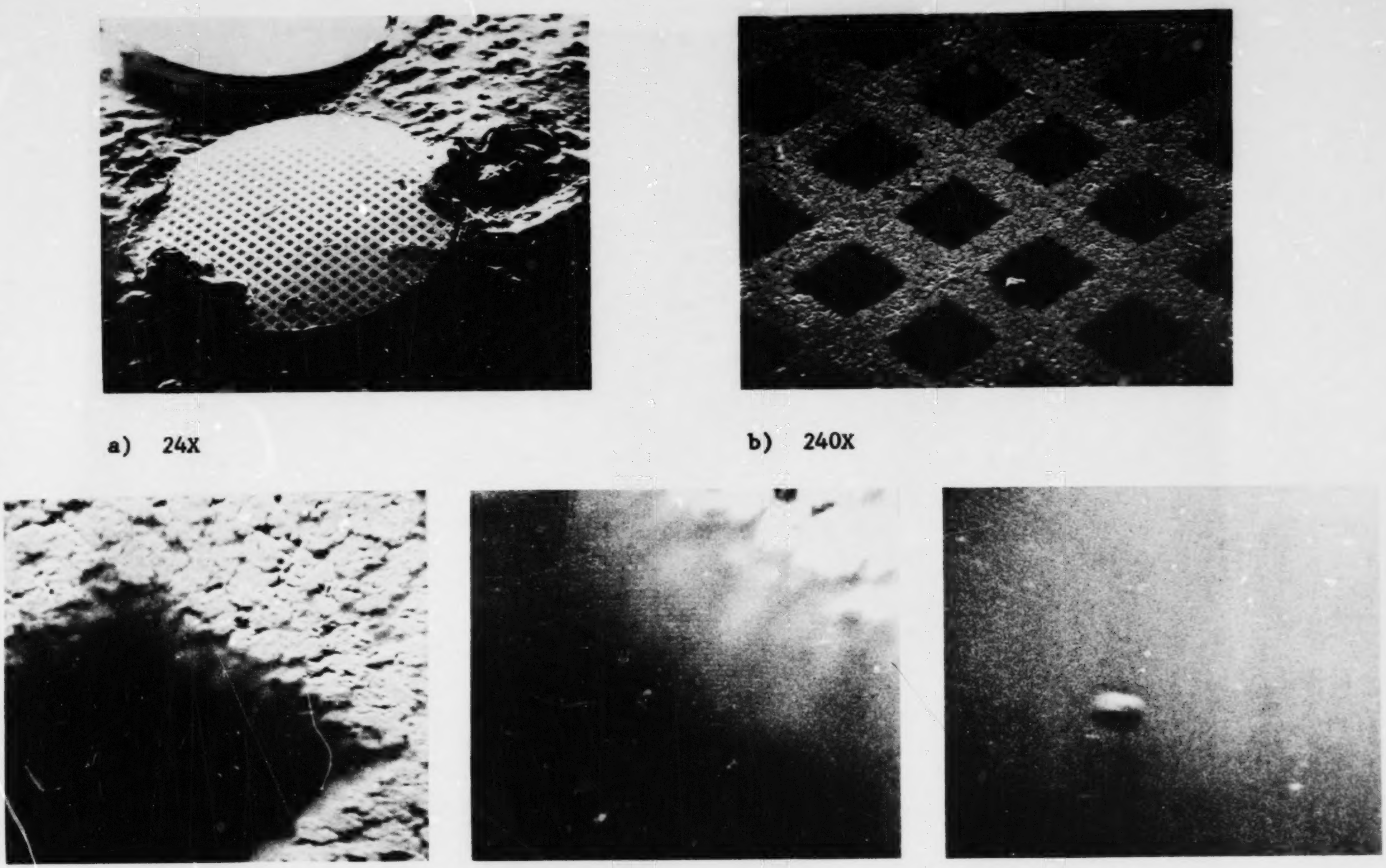

a) 24X

b) 240X

c) 1200X

d) 2400X

e) 6000X

Fig. 29 Scanning Electron Microscopy of Ni Film on Nitrocellulose
Stage 2

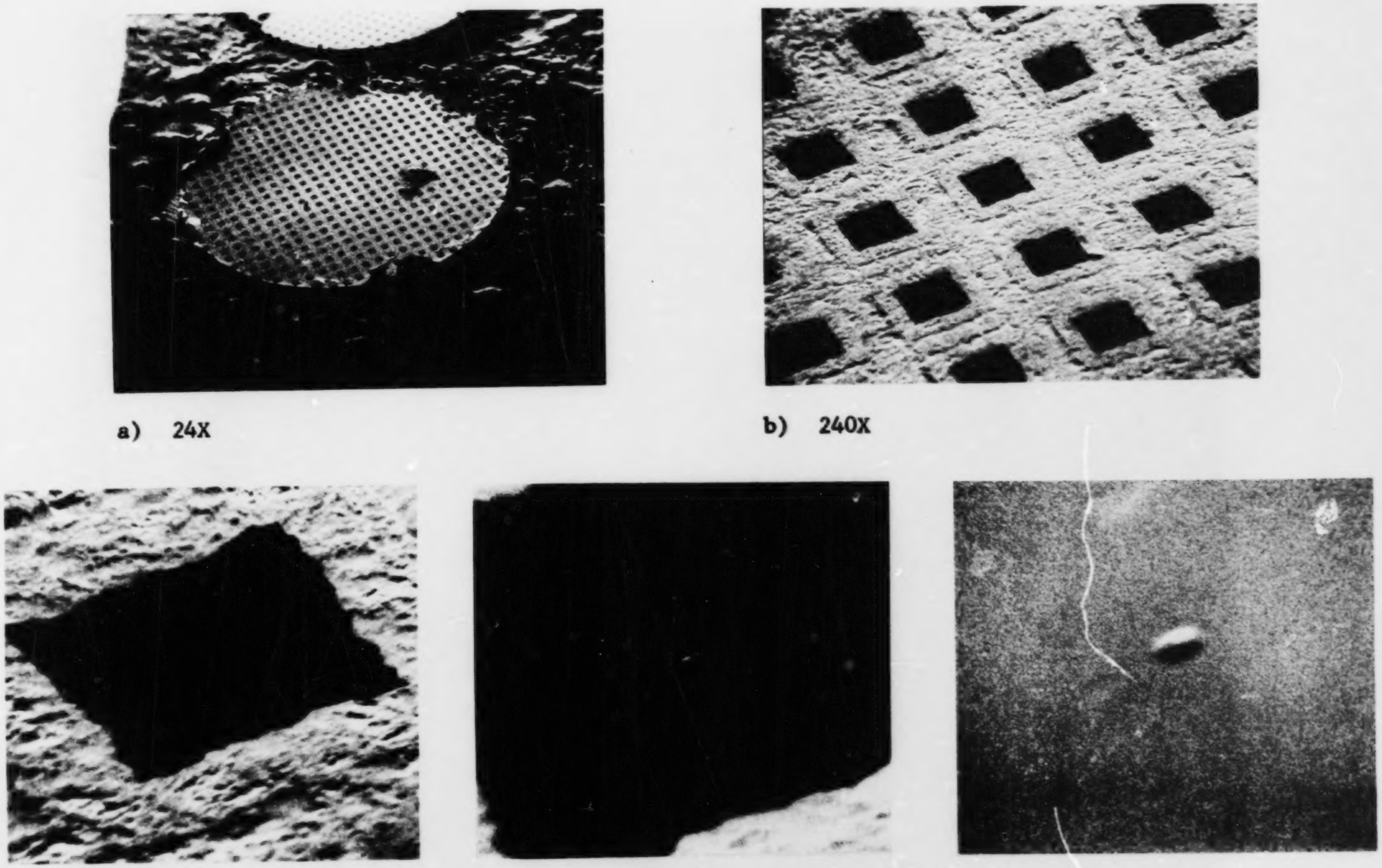

a) 24X

b) 240X

c) 1200X

d) 2400X

e) 6000X

Fig. 30 Scanning Electron Microscopy of Ni Film on Nitrocellulose

Stage 3

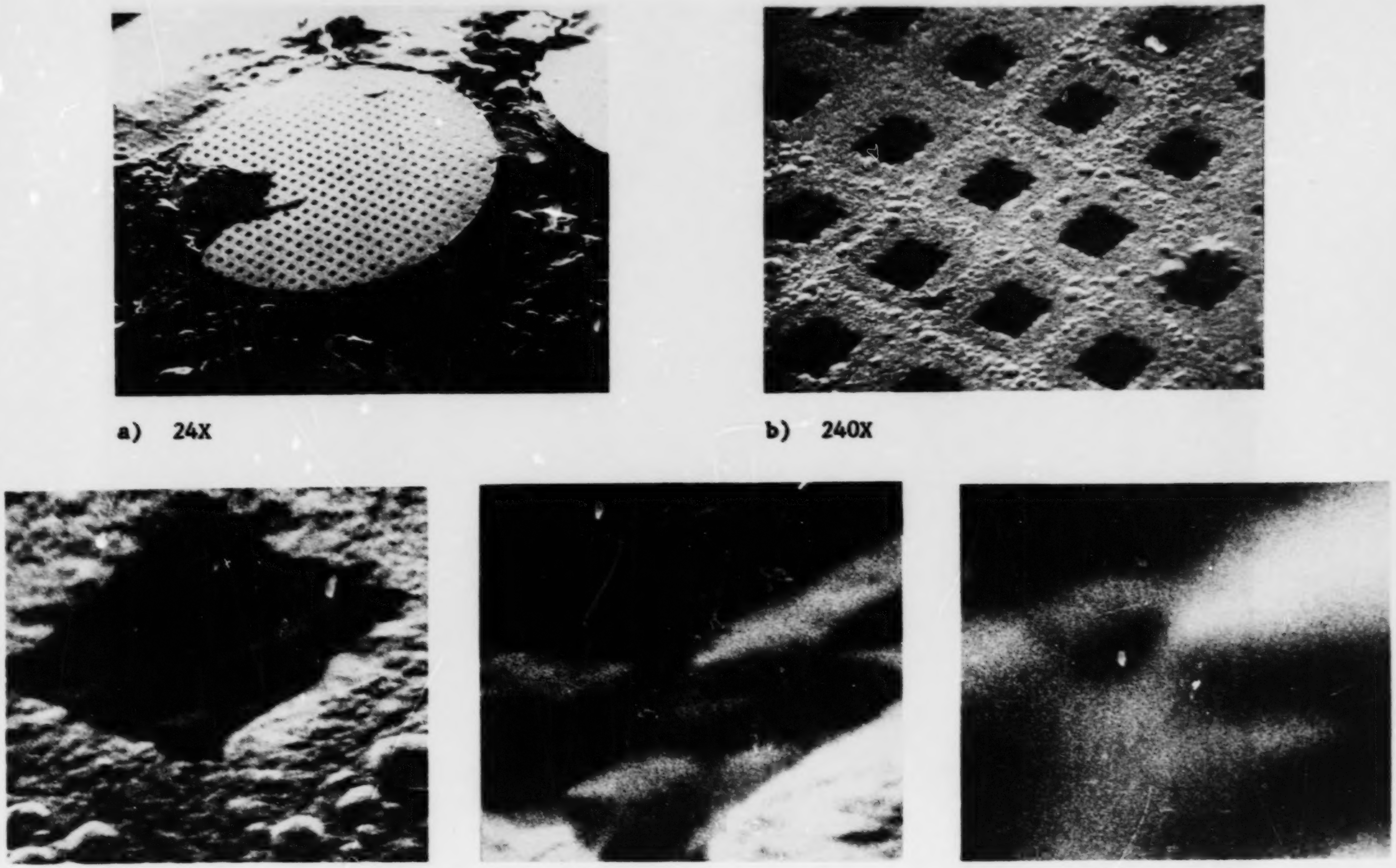

a) 24X

b) 240X

d) 1200X

e) 2400X

f) 6000X

Fig. 31 Scanning Electron Microscopy of Ni Film on Nitrocellulose
Stage 4

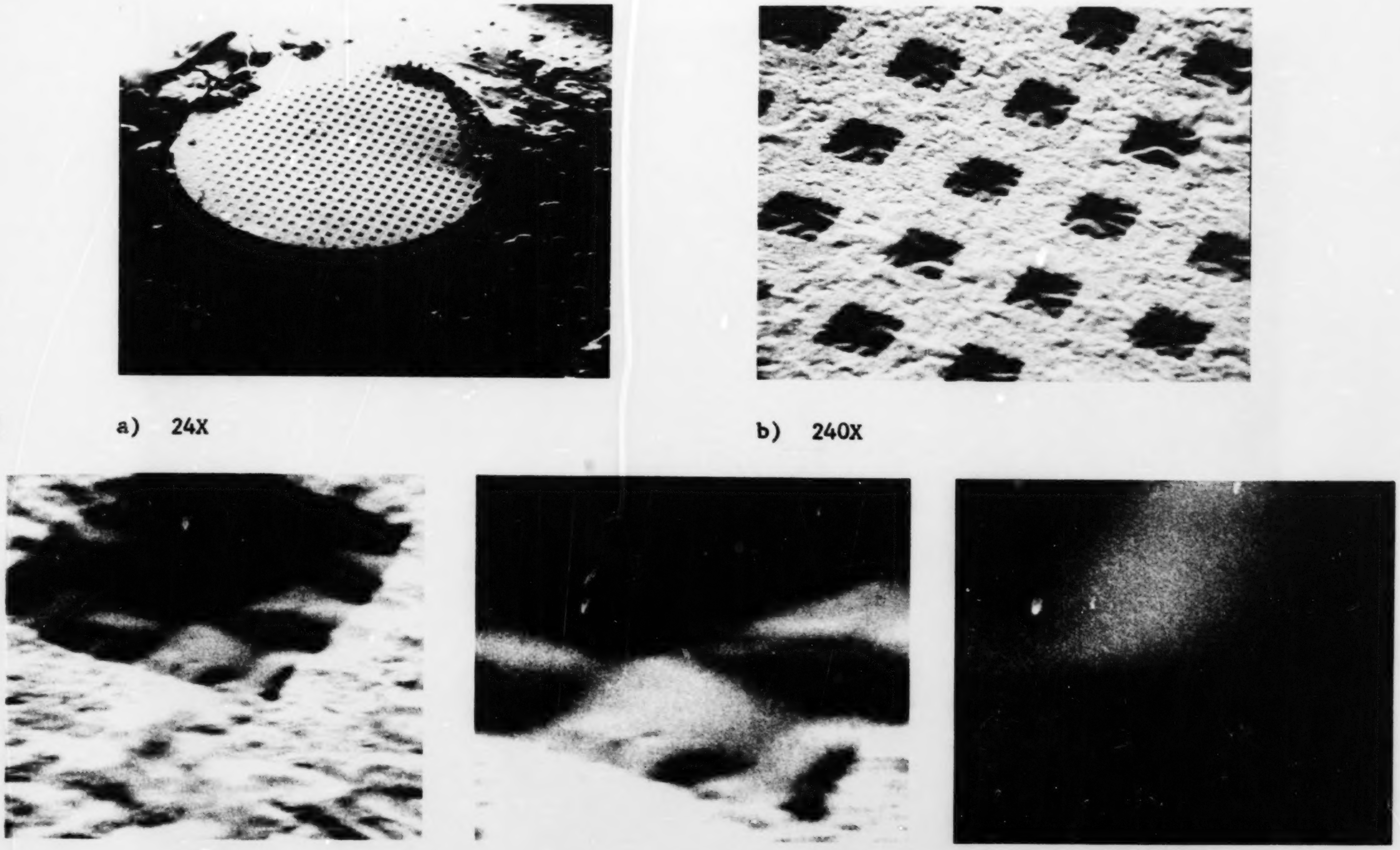

a) 24X

b) 240X

c) 1200X

d) 2400X

e) 6000X

Fig. 32 Scanning Electron Microscopy of Ni Film on Nitrocellulose

Stage 5

IV. Future Analytical Systems

The results of this work strongly indicate the type of instrumentation which would be necessary for small particle analysis.

The primary requisite in this analysis is that the capability of viewing the particles at relatively high magnifications (10,000X) be present. The superior ability of the Scanning Electron Microscope in furnishing topographical as well as morphological information suggests that the analytical capability should be built around this basic system.

Solid state Li drifted Ge detector systems are available from a number of manufacturers (Ortec, Princeton Gamma-Tech, etc.) which can be interfaced with the Scanning Electron Microscope to provide a non-dispersive detector system with less than 300 ev energy resolution, and analytical capability from Mg through U. These detector systems provide much better resolution than that available from conventional proportional detectors. In addition, recently developed linear spectrometer systems have been designed which have the capability of utilizing a much larger solid angle of x-rays than those employed for this study. These spectrometers, equipped with suitable crystals and thin detector windows, not only increase the x-ray intensity available for measurement but can also provide analytical capability for the light elements. In the final analysis, the analysis of small particles will still be limited by the volume of the particle to be analyzed. Since the x-ray intensity available from a particle is related to its volume (not its diameter) increasing the performance of a system such that an order of magnitude increase in x-ray intensity is realized will only extend the analytical capability of the system to particles which are one half the original size. These considerations would lead one to conclude that at present, the limiting particle size which can be analyzed by this technique is of the order of 0.1 microns.

References

1. S. Schur and R. E. Ogilvie, "Identification of Stratospheric Aerosols", AFCRL 62-99, January 1962.

2. C. Hemenway and R. Soberman, "Studies of Micrometeorites Obtained from a Recoverable Sounding Rocket". The Astronomical Journal, 67, June, 1962.

3. M. A. Schippert, S. H. Moll and R. E. Ogilvie, "Analytical Applications of a combined Electron Microscope/Electron Microanalyzer.

4. ASTM Special Technical Publication No. 349, "Symposium on X-ray and Electron Probe Analysis, American Soc. for Testing and Materials, 1963.

5. C. S. Barrett, "Structure of Metals", McGraw Hill New York Toronto London, p. 53, 1952.